EXTRATROPICAL CYCLONES

By J. BJERKNES

University of California, Los Angeles

Reprinted from the

COMPENDIUM OF METEOROLOGY

Published by the

AMERICAN METEOROLOGICAL SOCIETY

Boston, Massachusetts

This publication has been made possible through support and sponsorship extended by the Geophysics Research Division of the Air force Cambridge Research Center under Contract No. W 28-099 ac-399. It is published for technical information only and does not represent the recommendations or conclusions of the sponsoring agency.

EXTRATROPICAL CYCLONES

By J. BJERKNES

University of California, Los Angeles

With the consent of the editor the present article has been written as a summary of the research on extratropical cyclones in which the author himself has been directly involved. References to the work of others are therefore few, and the reader will not get a complete survey of the title subject.

This article is composed of two parts. In the first, extratropical cyclones are treated as simplified models for the sake of clarifying the theoretical principles. In the second, these principles are applied to a real storm over North America whose development may be considered as the prototype of a simple life history of extratropical cyclones. The modifications of that life history, caused by the varying initial conditions and the influence of neighboring systems in the general circulation, are treated by Dr. E. Palmén in his contribution to the Compendium.

DYNAMICS OF SIMPLIFIED CYCLONE MODELS

Theory of Pressure Changes and Thermal Structure of Extratropical Cyclones. The fully developed extratropical cyclone consists of a counterclockwise[1] vortex which extends upward into a wave trough in the upper westerlies. The dynamics of the extratropical cyclone is therefore a composite one, combining the dynamic phenomena of the vortex and the wave. We will here state separately the essential features of the atmospheric vortex and the atmospheric wave and then proceed to describe the composite dynamics of the extratropical cyclone.

In analyzing the displacement, intensification, and weakening of vortices and waves it is useful to consider the accompanying pressure changes, which obey the "tendency equation,"

$$\left(\frac{\partial p}{\partial t}\right)_h = -\int_h^\infty g \operatorname{div}_H (\rho \mathbf{v}) dz + (g\rho w_z)_h. \qquad (1)$$

Expressed in words, the rate of pressure change with time at a fixed point at the level h is determined partly by the net horizontal inflow into the vertical unit air column from h to the top of the atmosphere and partly by the vertical inflow of air through the base of that column.

A circular cyclonic vortex with vertical axis centered at the pole of a planet without mountains represents the simplest case of atmospheric vortex dynamics. In the case of frictionless motion in such a polar vortex the particles could be kept in steady-state zonal motion from west to east. The horizontal divergence is then everywhere zero and no vertical motion occurs, so that the tendency equation must indicate zero local pressure change at all points. With friction against the ground, the flow in the lowest part of the atmosphere would be given a component of indraft towards the vortex center, and this horizontal convergence of mass would make the pressure rise in the central portion of the pressure minimum, thus decreasing the zonal air motion. No steady state would be reached until the flow at the ground and the horizontal pressure gradient at the ground have reached zero. If the central core of the vortex is colder than its environment, there would still be a pressure gradient towards the pole in the free atmosphere, and there the air may continue its west to east circulation without horizontal divergence. This picture corresponds rather well to reality as represented by the time-averaged motion in the arctic region: almost zero meridional pressure gradient and zero zonal motion at the ground, and increasing poleward pressure gradient with height, accompanied by increasing westerlies with height. The initial assumption of a cyclone at the pole, and the additional assumption of friction at the ground, thus lead to the dynamical prediction that the cyclone at the ground should eventually disappear, while in the free atmosphere it should be conserved. This behavior of the circular cyclonic vortex can be generalized to apply also at other latitudes; the simple circular vortex is liable to die out gradually at the ground because of friction.

The circular cyclonic vortex centered in middle latitudes does not represent a steady-state dynamic system even in the absence of friction at the ground. Although the horizontal pressure gradient may everywhere be directed towards the center and its intensity may be a function only of the distance from the center, the motion around the center cannot be a simple circular one, because the Coriolis parameter varies from the northern to the southern part of the vortex. As a result of the variation of the Coriolis parameter the wind will be stronger in the southern than in the northern part of the vortex, and the net air transport across a north-south median wall will be from the western to the eastern half of the vortex. Consequently the pressure will rise in the eastern half because of horizontal convergence and fall in the western half of the low pressure system because of horizontal divergence, so that the pressure minimum and the accompanying vortex will drift westward. Eccentricity of the pressure field of such a sense as to involve a stronger pressure gradient in the southern than in the northern part of the vortex may reduce, neutralize, or even reverse that drift. The dynamic theory for the eccentric vortex has been developed in approximate form

1. All references to the sense of rotation in this article apply to the Northern Hemisphere.

by Holmboe [3]. He defined a "critical eccentricity" which would balance the exchange of air between the two halves of the vortex. Values of the quantity $|v| - |v'| - 2c = 4\Omega a\sigma_p^2 \cos\phi$, evaluated in a narrow isobaric channel of critical eccentricity, are given in Table I (v and v' are the wind velocities at southernmost and northernmost points, respectively, of the isobaric channel, c is the eastward speed of displacement of the vortex, Ω the angular speed of the earth, a the earth's radius, σ_p the angular radius of the isobaric channel, and ϕ the geographical latitude). In the case of the stationary vortex, the exchange of air between the eastern and western halves of the vortex is balanced if the wind velocity in the southernmost point of the isobaric ring exceeds that in the northernmost point by the tabulated amount. Near the center the flow can be almost constant all around the isobaric ring, but the greater the radius the more will the west wind in the south have to exceed the east wind in the north, particularly in low latitudes.

TABLE I. VALUES OF $|v| - |v'| - 2c = 4\Omega a\sigma_p^2 \cos\phi$ FOR CRITICAL ECCENTRICITY (in m sec^{-1})

ϕ	Angular radius of isobaric channel			
	1°	5°	10°	20°
90°	0	0	0	0
80°	0.1	2.5	9.9	—
70°	0.2	4.9	19.4	78
60°	0.3	7.1	28.4	114
50°	0.4	9.1	36.6	146
40°	0.4	10.9	43.6	175
30°	0.5	12.3	49.4	198

In applying the table to a moving vortex, twice the speed of displacement of the vortex must be added to the tabulated speed to give $|v| - |v'|$. For the eastward moving vortex the critical eccentricity is thus stronger than for the stationary one. Even slightly greater eccentricity would be needed to bring about accumulation of air in the western half of the pressure minimum and depletion of air in the eastern half, a condition which would seem necessary to make the system move eastward. A check with measured eccentricities shows, however, only "subcritical" cases; in other words all observed cyclonic vortices accumulate air in their front parts at the expense of the rear parts. The pressure change in such a moving vortex can therefore be explained only if other flow patterns prevail above the vortex. This conclusion is corroborated by the experience of synoptic aerology, and the typical upper flow pattern above moving vortices is that of the atmospheric wave. In the composite extratropical cyclone, the vortex part resists the eastward motion by piling up air in the front half; this resistance increases the faster the vortex is forced to move.

The atmospheric wave[2] superimposes a quasi-horizontal oscillation upon the fundamental current of straight westerlies. This is accompanied by a periodic distribution of horizontal mass divergence, which in first approximation depends on the relative strength of the "curvature and latitude effects" upon the wind speed. The curvature effect makes the air move supergeostrophically while overtaking the wave crest and subgeostrophically while overtaking the wave troughs. The latitude effect upon the wind speed comes from the fact that each flow channel is in a higher latitude at the anticyclonic bend than it is at the cyclonic bend, so that, the horizontal pressure gradients being equal, the geostrophic wind would be stronger at the cyclonic than at the anticyclonic bend. The result of

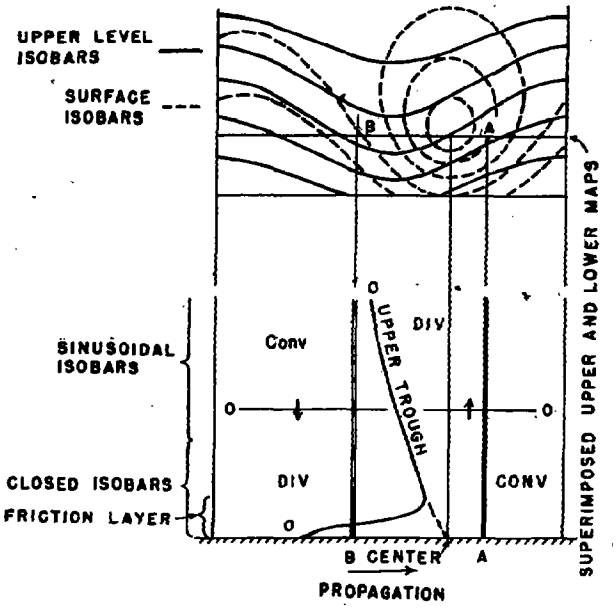

FIG. 1.—Schematic model of cyclone with lower-vortex and upper-wave part. West-to-east vertical profile shows location of horizontal divergence and convergence of mass.

these two opposite effects on horizontal divergence is in favor of the curvature effect when wave lengths are short and the fundamental current is strong. In this case the wave crests are preceded by horizontal convergence and the wave troughs by horizontal divergence. In the case of long waves and/or a weak fundamental current, the opposite distribution of horizontal divergence is established. The same conditions are found in air layers which move eastward more slowly than the wave.

In the usual baroclinic westerly current of middle latitudes a wave extending from the slow-moving lower layers to the fast-moving upper layers would have opposite patterns of horizontal divergence in the upper and lower part (see Fig. 1). At the level of transition between the upper and lower pattern a wave motion with zero horizontal divergence will exist. This "level of nondivergence" will be found at the height where the speed of the undisturbed current, v_z^*, is given by

2. The fundamental properties of the atmospheric waves of synoptic meteorology were first sketched by J. Bjerknes [2] and later developed mathematically by Rossby [26, 27] and Haurwitz [10]. In this article we follow the more recent treatment by J. Bjerknes and Holmboe [3].

$$v_x^* = c + \frac{2\Omega a \cos^3 \phi}{n^2}. \quad (2)$$

In this equation c is the eastward speed of propagation of the wave, Ω is the angular velocity of the earth, a is the earth's radius, ϕ is the geographical latitude, and n is the wave number per circumference of the earth. Numerical values of $(2\Omega a \cos^3 \phi)/n^2$ are given in Table II. This table, in conjunction with equation (2), shows that in short waves, such as are found to accompany the individual traveling cyclone, the level of nondivergence lies at an elevation where the undisturbed current moves only a little faster than the wave. In long waves the air at the level of nondivergence moves eastward much faster than the wave itself, particularly in low latitudes.

TABLE II. VALUES OF $(2\Omega a \cos^3 \phi)/n^2$ (in m sec^{-1})

ϕ	Wave length (deg. long.)				
	180°	120°	60°	36°	18°
70°	9.3	4.1	1.0	0.4	0.1
60°	29.0	12.9	3.2	1.2	0.3
50°	61.6	27.4	6.8	2.5	0.6
40°	104.3	46.3	11.6	4.2	1.0
30°	150.7	67.0	16.8	6.0	1.5

The level of nondivergence may be determined from sets of aerological maps, with the aid of Table II. Its height differs from case to case, but according to Charney [4] and Cressman [5] it averages around 600 mb for both long and short waves. Hence, with a given model of baroclinic westerlies, the speed v_x^* of the undisturbed westerlies at the level of nondivergence is approximately the same parameter for long and short waves. The speed of all such waves, which are superimposed on the same westerly current, therefore varies with wave length according to the formula,

$$c = v_x^* - \frac{2\Omega a \cos^3 \phi}{n^2}. \quad (3)$$

Short waves (large n) move almost with the speed of the air at the level of nondivergence. Long waves move eastward more slowly than short ones, and may also retrograde. Table II, applied to the case $c = 0$, gives us a survey of the wind at the level of nondivergence in stationary waves. At 70° latitude the west wind must be quite light for waves to be stationary, and the 180° wave length seems to be the most likely one for standing waves. Proceeding to lower latitudes, we find that the 180° stationary wave requires stronger westerlies than are ever known to occur. Assuming that v_x^* would never be greater than 30 m sec^{-1}, we see that below 60° latitude the 180° stationary waves would never occur, below 50° the 120° stationary waves also become impossible, and so on. This dependence of the long-wave pattern on geographical latitude usually leads to the establishment of only two or three standing waves per earth's circumference near the pole and stationary patterns with higher wave numbers in lower latitudes. In the latitudes of pattern transitions, complicated cases of wave interference occur.

The waves in the westerlies associated with the moving extratropical cyclones are by necessity of short wave lengths, say thirty degrees longitude. According to (3) and Table II, such waves move with a speed c, only slightly smaller than v_x^*, the speed of the westerlies at the level of nondivergence.

Figure 1 shows the position of the pressure minimum at sea level relative to that of the upper trough. The axis of minimum pressure of the closed low tilts towards the coldest side, which is usually to the west or northwest of the location of the surface center. The tropospheric part of the upper trough is also displaced westward with height, but not as far per unit height as the subjacent center of low pressure.

The friction layer of the closed vortex (up to about 1-km height) has horizontal convergence. Above the influence of surface friction the eastern half of the vortex has horizontal convergence of mass and the western half, horizontal divergence. This holds true also for the upper trough up to the level of nondivergence, beyond which divergence and convergence exchange positions. The tendency equation (1) applied to the schematic cyclone cross section of Fig. 1 gives an answer to the two questions: How can the cyclone move eastward as most middle latitude cyclones do? and, How can it deepen despite the frictional convergence?

The eastward displacement of the cyclone is assured if the vertical integral of horizontal mass divergence in the tendency equation is determined as to sign by the atmosphere above the level of nondivergence. The deepening of the pressure minimum likewise depends on the influence from above the level of nondivergence. Because of the westward tilt of the axis of the cyclone a vertical air column located at the surface center will show horizontal convergence in its lower portion, where it passes through the forward part of the vortex, and horizontal divergence where it traverses the upper wave pattern east of the wave trough. Deepening of the surface center will occur only if this upper-air divergence overcompensates the low-level convergence.

In all parts of the cyclone the surface pressure tendency represents a small change in the weight of the local vertical column, resulting from the difference between accumulation and depletion of air, each of which represents much greater weight changes. The natural adjustment of the pressure tendencies to the observed moderate values can be visualized as follows. In the low-level vortex, the convergence in the front and the divergence in the rear are more strongly developed the faster the vortex is forced to move. We have also seen from Table II that the level of nondivergence in the upper wave rises to a higher elevation, and the divergence values above that level decrease, when the wave speed increases. Therefore, a supposed increase in speed without a change in the structure of the cyclone would lead to a weakening of the high-level contribution and a strengthening of the low-level contribution to the change in weight of air columns. This would be tantamount to a decrease in pressure tendencies. Quite analogously, it can be shown

that a supposed slowing down of the cyclone without change in its structure would lead to increasing surface pressure tendencies. From this it can be concluded that the speed of a given cyclone is stable as long as its total three-dimensional structure remains the same. The pressure tendencies are then also stable although they are made up as small differences of large opposite contributions of horizontal divergence and convergence.

A real increase in the divergence effects of the upper wave would come from a lowering of the level of nondivergence and an inherent increase of that part of the atmosphere in which the air current is supercritical. According to (3), this may take place through one of the following changes of parameters in the upper wave: (1) an increase of the speed v_x of the upper westerlies, (2) a decrease of angular wave length $2\pi/n$, and (3) travel towards higher latitudes. In all these cases the compensating mass-divergence effects from low levels automatically become greater as the speed of the cyclone increases. The occurrence of excessive values of barometric tendencies is thus automatically avoided.

The slowing down which is normally observed in deep and extensive cyclones is associated with the great depth of atmosphere moving in a closed cyclonic flow pattern. If that pattern has a subcritical eccentricity, which is the more frequent case, it will maintain mass convergence in the eastern half and mass divergence in the western half. The influence of an upper wave pattern can then only barely overcompensate the divergence effects below, and the resulting pressure tendencies will be small. A final reversal of tendencies, and a retrograding of the cyclone, will result if the low-level mass-divergence effects overcompensate those from the upper wave pattern.

The distribution of horizontal divergence also determines the vertical motion, which in the "smoothed" cyclone model always goes upward in the front half and downward in the rear (Fig. 1). This model feature agrees with the observed distribution of cloudiness and precipitation in the cyclones. Modern aerological analysis of the field of vertical motion carried on by the Department of Meteorology at New York University has corroborated these findings. A summary of the careful and extensive work in that field was published in 1948 by Miller [20]. From that report we also know that the vertical motion of extensive air masses usually is less than 3 cm sec^{-1} even at the level of nondivergence, where the maximum upward and downward values of momentum occur. Higher values of vertical motion up to 10 cm sec^{-1} should occur over narrow zones near fronts, while the occurrences of updrafts and downdrafts of several meters per second are restricted to small parts of individual convective clouds.

Typical patterns of temperature distribution in the extratropical cyclone can be seen from the sample cyclones described later in this article. The most frequent development of the temperature pattern in the lower tropospheric part of the vortex can be represented schematically by the maps and profiles in Fig. 2. The incipient cyclone (Fig. 2*a*) coincides with the apex of a warm tongue formed on a "front" across

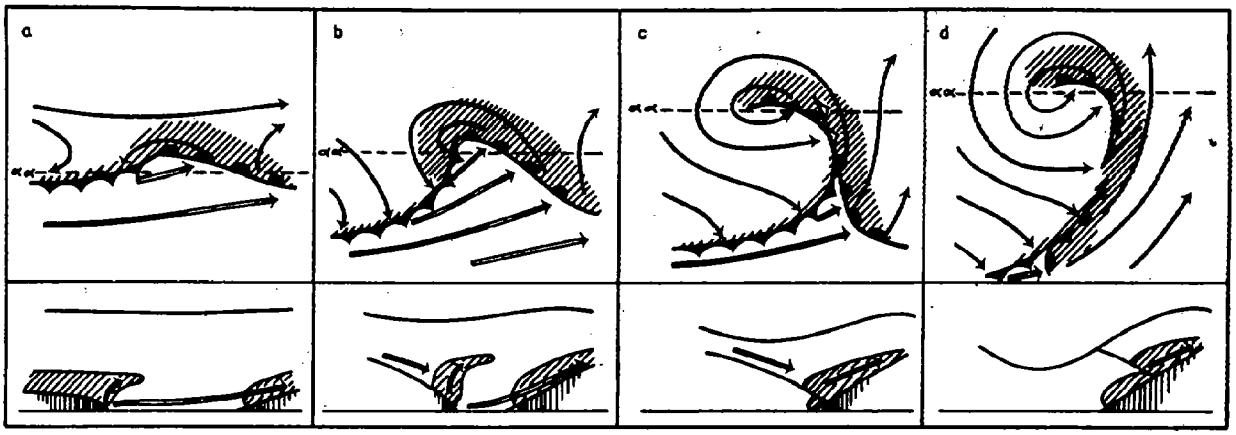

FIG. 2.—Successive stages of development of a frontal wave to an occluded vortex.

which the horizontal temperature gradient reaches a maximum. The frontal surface rises towards the cold side at an angle of inclination averaging around one in a hundred. It conserves its identity from day to day and moves along at a speed determinable from the winds through the kinematic boundary condition. The wave amplitude increases as the cyclone matures (Fig. 2*b*) and the central pressure decreases. Next follows the "occlusion" process (Fig. 2, *c* and *d*) during which the warm tongue is lifted from the ground, first near the center, later also farther out. The occluded front formed at the junction of the two cold wedges tends to wrap around the cyclone center as part of a spiral, and the same shape is found for the warm tongue in all levels of closed cyclonic circulation. In the profile in Fig. 2*c*, which is placed at a short distance south of the cyclone center, the occluded front is a warm-front type, that is, the cold wedge behind the occlusion is less cold than the one in front. This is also true of Fig. 2*d*, but it can usually be assumed that farther south the occlusion is a cold-front type. Where the transition from one occlusion model to another takes place the occluded front on the map must show a little

gap. The lifting of a tongue of warm air relative to a colder environment, illustrated in Fig. 2, can be assumed to furnish a great part of the increase in kinetic energy during the cyclonic development from wave to vortex.

The tropopause is also shown in the profiles. It has a crest over the warm-front surface and a trough over the cold-front surface, and the amplitude of the tropopause oscillation increases with the growth of the cyclone. In Fig. 2*d* the tropopause has a deep depression almost coinciding with the cyclone center, which is at that stage surrounded by air of cold origin up through the whole troposphere. Details of tropopause structure, such as the frequent subdivision into multiple tropopauses, have been left out in Fig. 2.

Hatched areas in Fig. 2 indicate the location of the main precipitation areas of the cyclone. The largest area is covered by the warm-front rain, where the air from the warm tongue climbs the receding wedge of cold air and condenses much of its moisture. A more narrow zone of precipitation accompanies the cold front where some air from the lower part of the warm tongue is lifted by the advancing cold wedge. Higher portions of the warm tongue move faster than the cold-front wedge and are not lifted by it. The described upward motion of the warm air next to the frontal surfaces should be visualized as being superimposed on the general pattern of vertical motion, upward in the front half and downward in the rear half of the cyclone (Fig. 1). This general, upward motion is sometimes sufficient to cause rain where it is not called for as a consequence of upgliding on frontal surfaces. Some extensive warm-sector rains and also the rain in the front half of a cold trough or a cold vortex are probably to be explained by the general upward motion shown in Fig. 1.

To complete the precipitation picture of the cyclone the air-mass precipitation should also be added, that is, the drizzle in the warm moist parts, caused by condensation from low clouds formed by the cooling of the warm air over cold surfaces (mainly ocean surfaces), and the convective showery precipitation formed through the heating from the ground, or through lifting of convectively unstable air at fronts.

While the thermal pattern of the cyclone near the ground is the result mainly of horizontal advection and nonadiabatic gain or loss of heat exchanged with the ground, the pattern in the free atmosphere is also influenced by the slow but systematic vertical displacement of the air shown in Fig. 1 and by the heat transfer of penetrative convection. However, the dominant process for the shaping of the upper-tropospheric temperature field is horizontal advection. The development of the thermal pattern of the waves in the upper westerlies follows roughly the advective scheme shown in Fig. 3. A warm tongue forms in the part of the wave with advection from the south, and a cold tongue in the part with advection from the north. In this early stage of the wave the pressure crests and troughs must tilt westward, as shown for the pressure trough in Fig. 1. In the further development, both warm and cold tongues grow in amplitude and move forward relative to the pressure wave, because the eastward motion of the air exceeds that of the wave. If the wave motion were entirely horizontal, a thermal pattern of permanent structure relative to the moving wave would be reached when the isotherms have adapted to the shape of the relative streamlines. For the idealized case of v_x = constant in each level of the sinusoidal

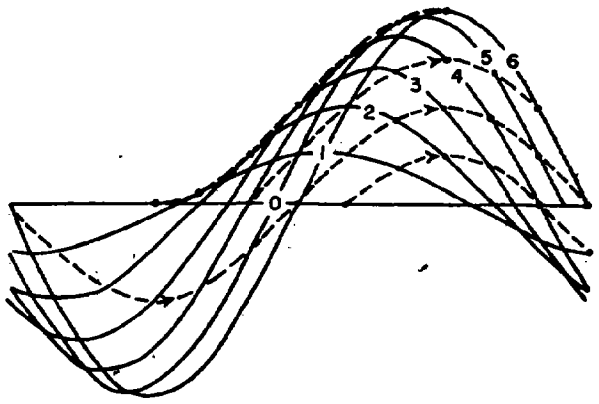

FIG. 3.—Advective formation of the thermal upper wave by the winds blowing relative to the moving pressure wave.

wave pattern, the ratio of the amplitude A_R of the relative streamline to that of the streamline A_S would be

$$\frac{A_R}{A_S} = \frac{v_x}{v_x - c}. \tag{4}$$

Hence, close to the level where v_x is equal to the wave speed c, the relative streamlines, and with them the advectively transported isotherms, would acquire a much greater amplitude than that of the streamline. The ratio A_R/A_S will decrease from that level upward to the tropopause, where v_x has its maximum.

Under the influence of the upward motion ahead of the pressure trough and downward motion behind it, the ratio in (4) would be reduced, as shown by Miller [20]. Synoptic experience shows that A_R/A_S stays positive in all tropospheric levels where $v_x > c$, also under the joint influence of vertical motion and horizontal advection. In other words, after a period of thermal transformation of the type shown in Fig. 3, the waves in the upper troposphere tend to become thermally symmetric, with warm tongues coinciding with pressure crests and cold tongues with pressure troughs.

With the reversal of the meridional temperature gradient from troposphere to stratosphere, the advective effects on temperature in the upper waves are also reversed. Hence the stratospheric pressure crests are cold and the pressure troughs warm. It then follows indirectly that the wave pattern of pressure crests and troughs rapidly loses amplitude with height in the stratosphere. In the stably stratified stratosphere the local warming and cooling through vertical motion are stronger than in the troposphere, and are quite

often stronger than the temperature change by advection.

Vorticity Analysis of the Extratropical Cyclone. An analysis of the vorticity distribution and the history of vorticity change of individual parcels in the vortex and wave will reveal more of the dynamics of the cyclone. The vertical component of the vorticity ζ may be identified on the horizontal streamline maps as a particle rotation about a vertical axis, partly due to curvature, v/r_s, where r_s is the radius of curvature of the streamline, and partly due to shear, $-\partial v/\partial n$:

$$\zeta = \pm \frac{v}{r_s} - \frac{\partial v}{\partial n} = \frac{\partial v_y}{\partial x} - \frac{\partial v_x}{\partial y}. \qquad (5)$$

The rules for determining the algebraic sign can always be decided upon by referring to the Cartesian component form of vorticity, added as an alternate expression in (5). The convention used here is to let the positive direction of the coordinate n point to the left of the wind, to consider v and r_s always positive, and to use the positive sign in front of v/r_s for cyclonic and the negative sign for anticyclonic curvature of the streamlines.

The vorticity change of the individual traveling particle [11, 13, 16, 26, 27] is given by the equation,

$$\frac{d\zeta}{dt} = \frac{\partial p}{\partial x}\frac{\partial \alpha}{\partial y} - \frac{\partial p}{\partial y}\frac{\partial \alpha}{\partial x} - (\zeta + 2\Omega \sin\phi)\,\mathrm{div}_H\,\mathbf{v} - \frac{(2\Omega\cos\phi)}{a}v_y + \frac{\partial v_z}{\partial y}\left(2\Omega\cos\phi + \frac{\partial v_x}{\partial z}\right) - \frac{\partial v_z}{\partial x}\frac{\partial v_y}{\partial z}. \qquad (6)$$

The first two terms on the right represent in component form the effect of isobaric-isosteric solenoids on the change of vertical vorticity. These terms are always found to be insignificant compared to the following ones. The divergence term shows how horizontal expansion (divergence) creates negative (anticyclonic) vorticity, and horizontal contraction creates positive (cyclonic) vorticity. The next term shows the effect on relative vorticity ζ of the displacement of the air, either towards the polar regions where the vertical component of the earth's vorticity $2\Omega \sin\phi$ is great, or towards the equator where $2\Omega \sin\phi$ is zero. In the absence of the other factors, poleward movement would entail a decrease of relative cyclonic vorticity or an increase of relative anticyclonic vorticity, and movement away from the pole would entail an increase of relative cyclonic vorticity or a decrease of relative anticyclonic vorticity. The last two terms on the right-hand side describe the influence of the vertical motion in changing the vorticity about the vertical. The term involving $\partial v_z/\partial y$ represents, in part, the fact that the infinitesimal disk of air, whose rotation decides the value of ζ, arrives at a horizontal position from earlier positions with meridional tilt. In terms of relative-vorticity change, this is equivalent to a change in latitude in addition to that by horizontal meridional advection, as can be seen from the analogy between the terms $(2\Omega\cos\phi)\partial v_x/\partial y$ and $-(2\Omega\cos\phi)v_y/a$. Furthermore, the term in $\partial v_z/\partial y$ represents the effect of rotating the air in the yz-plane so that the vorticity about the y-axis, $\partial v_z/\partial z$, acquires a vertical component at the rate $(\partial v_z/\partial y)(\partial v_z/\partial z)$ per unit time. Analogously, the last term in (6) represents the rate of change of vorticity about the z-axis resulting from a rotation of the air in the xz-plane. Usually the terms in $\partial v_z/\partial y$ and $\partial v_z/\partial x$ are considered to be insignificant in relation to the divergence term and the meridional advection term, but possible exceptions will be mentioned below.

In the frontal wave of the lower troposphere, the cold air enters the moving cyclone along the warm front (Fig. 4). Near the front it has initial cyclonic shear

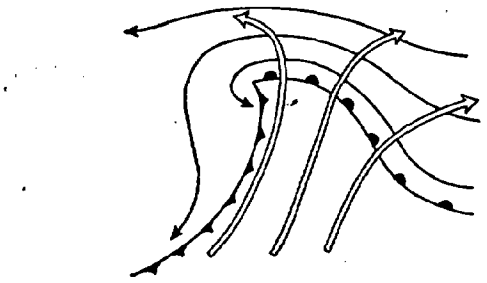

FIG. 4.—Motion of warm and cold air relative to the moving frontal wave.

which had been acquired during the period of frontogenesis (see p. 590). The increase of the cyclonic vorticity in the cold air on its way toward the wave apex is due to the horizontal convergence, which extends all over the front half of the cyclone (see Fig. 1). This creation of relative cyclonic vorticity is somewhat reduced by the effect of the poleward component of air travel. Behind the wave apex the air returns southward and as a result its relative cyclonic vorticity should increase. At the same time, however, the air enters the region of horizontal divergence, which has the opposite effect upon vorticity change. The result is that the air which had acquired maximum cyclonic shear along the warm front maintains cyclonic vorticity after passing the wave apex, but with a simultaneous shift from shear to curvature vorticity. The cold air passing at greater distance from the center changes from moderate cyclonic to anticyclonic vorticity. During the growth of the cyclone more and more of the cold air is able to maintain its cyclonic vorticity after passing the wave apex.

The warm air in the frontal wave enters the cyclone from the southwest. Its speed in lower levels just barely exceeds that of the cyclone in its eastward motion. Upon arrival at the warm front the warm air climbs the receding cold wedge. Again, one branch of anticyclonic and another of cyclonic vorticity may be discerned. Farthest away from the center, where the horizontal convergence is moderate or nonexistent, the warm air gains anticyclonic relative vorticity through the poleward component of movement. Closer to the center, where the horizontal convergence is stronger, the warm air acquires cyclonic relative vorticity despite its dis-

placement polewards. This latter development, which does not start until the cyclone is past the nascent stage, gains in magnitude with the growth of the cyclone.

In the westerly wave of the upper troposphere, as represented in Fig. 1, the air enters the cyclone from the northwest and leaves it toward the east, across the wave crest ahead of the surface cyclone. As long as the upper wave does not degenerate, the relative vorticity changes sign at the longitude of the inflection points, thus changing from anticyclonic to cyclonic relative vorticity in the middle of the upper zone of convergence, and from cyclonic to anticyclonic in the middle of the upper zone of divergence. This vorticity change by divergence is supported by the effect of meridional advection.

The factor ($\zeta + 2\Omega \sin \phi$) in the divergence term of (6) is equal to the absolute vorticity ζ_a of the air relative to a nonrotating coordinate system. When ζ is positive (cyclonic), ζ_a is large and the individual vorticity change with time becomes quite sensitive to horizontal convergence or divergence. If the air is subject to a sustained process of horizontal convergence, its cyclonic vorticity will increase without any theoretical upper limit. The cyclonic bends of an upper sinusoidal westerly are therefore frequently seen to become strongly curved. On the other hand, when ζ acquires large negative (anticyclonic) values, the absolute vorticity may go to zero or even become negative. This happens almost exclusively in the upper troposphere and lower stratosphere where the wind velocities are very strong. On wave crests where ζ_a reaches values close to zero, the vorticity change is only feebly influenced by horizontal divergence, and obeys mainly the term of meridional advection in (6). This would be equivalent to motion under approximately constant absolute vorticity $\zeta_a \approx 0$ or $\zeta \approx -2\Omega \sin \phi$. If a wave crest in the upper atmosphere has developed to that extreme stage, the particles overtaking the crest would maintain their anticyclonic vorticity (in the form of curvature and/or shear) for a long period thereafter. Figure 5 illustrates that case schematically. From an initial flow pattern of sinusoidal westerlies (streamline 1) a "meandering" westerly current develops through the growth of the wave crest and the deepening of the next downwind wave trough (streamlines 2 and 3). This development towards meandering flow is not dependent on the absolute vorticity's actually having reached zero. With absolute vorticities still positive, but numerically small, the vorticity change begins to react sluggishly to horizontal convergence with the result that the sinusoidal perturbation of the westerlies begins to degenerate. The meandering development may also start from an initially straight current with anticyclonic shear close to the value $-2\Omega \sin \phi$. Any small wave impulse may then develop into meandering wave patterns.

It is obvious that the meandering phenomenon, once started in regions of excessive anticyclonic vorticity in the upper atmosphere, will also have a profound influence on the total cyclone picture down to the ground. The deepening of the upper wave trough is associated with the deepening of the cyclonic vortex underneath, and usually also entails a southward component added to the normal eastward displacement of the cyclone. In all cases of such deepening the initial upper disturbance must start through the build-up of excessive anticyclonic curvature on the wave crest to the west of the cyclone. Above the level of nondivergence, the divergence term and the meridional advection term in (6) are of the same phase, so that the additional terms in $\partial v_s/\partial y$ and $\partial v_s/\partial x$ are not likely to affect the general pattern of $d\zeta/dt$ very much. The two levels where their influence may be expected to count are (1) close to the level of nondivergence, and (2) at the localities where

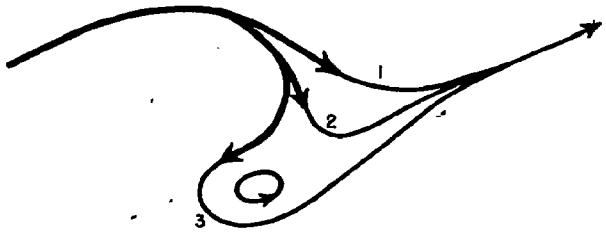

FIG. 5.—Successive (1→ 3) degeneration of sinusoidal wave-pattern caused by excessive anticyclonic vorticity on wave crest.

$\zeta - 2\Omega \sin \phi$ is near zero. In both cases the competition with the divergence term is almost eliminated. Furthermore, v_s and its horizontal derivatives reach their maximum in the upper troposphere (about two kilometers above the level of nondivergence where $|\rho v_s|$ has its maximum).

The most compelling reason for admitting a perceptible influence of the terms in $\partial v_s/\partial y$ and $\partial v_s/\partial x$ on the variations of ζ lies in the fact that neither the divergence term, nor the meridional advection term, nor their sum, can account through equation (6) for the occurrence of negative absolute vorticity. Analyses of observational data do show areas of negative absolute vorticity on pronounced upper wave crests and/or south of pronounced "jet streams" (see Fig. 7). A vertical motion effect of the right sign to explain the growth of $-\zeta$ beyond $2\Omega \sin \phi$ would be found north of the maximum of upward velocity in the cyclone ($\partial v_s/\partial y < 0$, $\partial v_s/\partial z > 0$). The result in terms of a large anticyclonic vorticity, and occasionally a negative absolute vorticity, can then be expected to accrue on the upper wave crest to the east of the cyclone.

The above reasoning about the vertical motion terms in equation (6) has been developed by L. Sherman and will appear under his authorship.

Inertial Motion in Isentropic Surfaces. In slow-moving long waves of the upper westerlies, the streamlines relative to the waves almost coincide with the streamlines relative to the earth, and the isotherms will be moved advectively so as to coincide more or less with the isobars. Around the inflection points of such long waves we find the best approximation to the relatively simple conditions of straight baroclinic flow. Frontogenesis and frontal cyclogenesis are frequent

under the straight southwesterly currents of long waves, and for a study of these phenomena we will here consider the theory of adiabatic, inertial motion in tilting, stationary isentropic surfaces. Adiabatic (or pseudo-adiabatic) changes of state of particles in the free atmosphere can justifiably be assumed, because non-adiabatic temperature changes are so slow and uniformly distributed that they do not appreciably affect a relatively rapid phenomenon such as cyclogenesis.

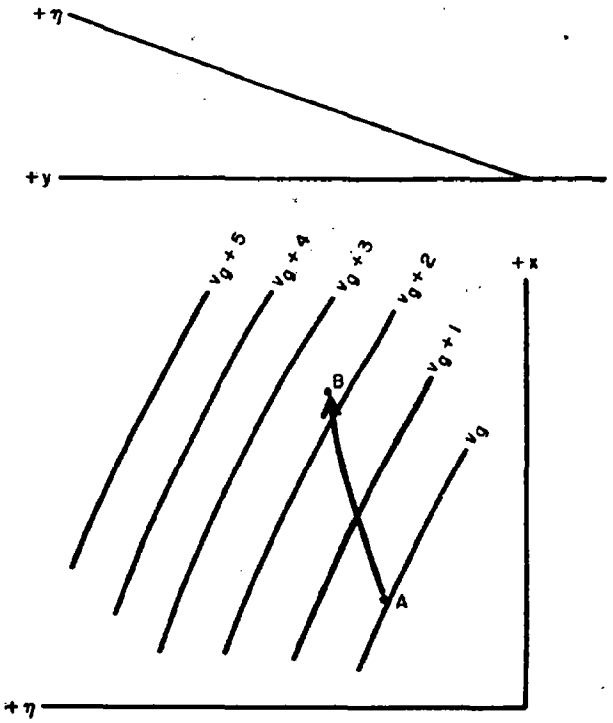

FIG. 6.—Profile of sloping isentropic $x\eta$-plane and sample distribution of the isovels of v_g in $x\eta$-coordinates.

The following simplified analysis has been inspired by the theoretical studies on "dynamic instability," which go back to the classical paper of Helmholtz, "Über atmosphärische Bewegungen," published in 1888 [12]. Several recent contributions by theoretical meteorologists to the same field have been included in the list of literature references [6–9, 14, 15, 17–19, 21, 31, 32]. The synoptic applications of equation (11) in this article to the problems of frontogenesis and cyclogenesis have, to my knowledge, not been attempted before.

The adiabatic movement of a particle parallel to an isentropic surface (sloping or horizontal) is not opposed by buoyancy forces and is left to the stable or unstable control of the horizontal pressure gradient and the Coriolis force. The same is true for particles of entire isentropic sheets moving in unison, when they are far enough from the ground to be independent of boundary effects. For the purpose of this article we shall consider the environmental field of pressure and potential temperature constant while the sample particle (or sample isentropic sheet) moves isentropically through the field. We shall consider part of an isentropic surface of sufficiently small extent to be treated as a sloping plane (Fig. 6), on which the horizontal direction will be called the x-direction (due eastward) and the direction of steepest slope (due northward) will be called the η-direction. The η-axis is supposed to form an angle with the horizontal y-axis of the order of one in a hundred or less. The undisturbed air motion is supposed to be zonal, geostrophic, and horizontal, which allows the isentropic surface to stay fixed in space. Furthermore the fundamental motion is constant along each streamline, $\partial v_x/\partial x = 0$, and represents a steady state, $\partial v_x/\partial t = 0$. Later application to the long wave, where the quasi-straight flow is not exactly zonal, will be done without any strict mathematical treatment. The disturbed motion of the sample particle is supposed to be contained in the isentropic surface and to have an initial upslope component v_η superimposed on the general horizontal motion characteristic of the environment.

The x-component of acceleration of the disturbed particle amounts to

$$\frac{dv_x}{dt} = 2\Omega_z v_y \cong 2\Omega_z v_\eta, \tag{7}$$

and makes the particle speed up in the positive x-direction while it climbs the isentropic slope. The wind of the environment v_g, which is geostrophic and directed along the x-axis in the whole field, changes in value along the path of climb. An observer following the disturbed particle would see the environmental geostrophic wind, relative to the earth, change by

$$\frac{dv_g}{dt} = v_\eta \frac{\partial v_g}{\partial \eta}. \tag{8}$$

The x-component of the speed of the disturbed particle was assumed to be equal to the geostrophic wind v_g at the initial time. Depending on whether $dv_x/dt > dv_g/dt$ or $dv_x/dt < dv_g/dt$, the disturbed particle will move eastwards faster or slower than its new environment after a time differential of climbing. In the first case, the y-component of acceleration of the disturbed particle $dv_y/dt = -2\Omega(v_x - v_g)$ will be directed down the isentropic slope opposite to the initial disturbance. A stable inertia type of oscillation will then result. In the second case, the y-component of acceleration will point in the same direction as the initial disturbance velocity v_η, so that an exponential growth of the disturbance will follow. The instability case is thus $dv_x/dt < dv_g/dt$. In order to make the instability criterion applicable also for the downward directed disturbance, it should be written $\left|\frac{dv_x}{dt}\right| < \left|\frac{dv_g}{dt}\right|$.

Now, provided that the substitution of v_η for v_y in (7) is justified by a sufficiently small inclination of the isentropic surface, the instability criterion derived from (7) and (8) takes the simple form,

$$\frac{\partial v_g}{\partial \eta} > 2\Omega_z. \tag{9}$$

The observed increase of westerly geostrophic wind from the lower to the higher portion of an isentropic

surface sometimes satisfies this instability criterion, as will be shown later.

If we drop the initial conditions of $\partial v_x/\partial x = 0$ and $\partial v_x/\partial t = 0$, no exact treatment can be offered, because then the fundamental current is not a steady-state one. The following reasoning should however be valid, provided that the long-wave deformations of the fundamental current are much slower than the short-wave developments on the isentropic surface. This condition is usually fulfilled.

In Fig. 6 an element of the isentropic surface is shown in $x\eta$-coordinates. Isobars on that surface are parallel to the x-direction, while the distribution of the speed of the geostrophic wind v_g is shown by slanting scalar curves. Thus v_g has a gradient in the x-direction in addition to the much stronger gradient in the η-direction. The disturbed path of a sample particle along the isentropic surface is supposed to go from A to B during the time differential. The x-component of the acceleration (parallel to the isobars) of the sample particle is again, to a first approximation, $dv_x/dt = 2\Omega_z v_\eta$, while the change of geostrophic wind encountered along the path is

$$\frac{dv_g}{dt} = v_\eta \frac{\partial v_g}{\partial \eta} + v_x \frac{\partial v_g}{\partial x} + \frac{\partial v_g}{\partial t}. \tag{10}$$

The acceleration of the particle in the η-direction is supposed to be zero at the initial point of the trajectory A. The acceleration in the η-direction will also be zero at the end of the trajectory B if $dv_x/dt = dv_g/dt$, or

$$2\Omega_z v_\eta = v_\eta \frac{\partial v_g}{\partial \eta} + v_x \frac{\partial v_g}{\partial x} + \frac{\partial v_g}{\partial t},$$

that is,

$$v_\eta = \frac{v_x \dfrac{\partial v_g}{\partial x} + \dfrac{\partial v_g}{\partial t}}{2\Omega_z - \dfrac{\partial v_g}{\partial \eta}}. \tag{11}$$

Specializing now for the condition $2\Omega_z - \partial v_g/\partial \eta > 0$ and for $v_x \partial v_g/\partial x + \partial v_g/\partial t > 0$, we find that the particle given an initial speed component v_η greater than the value found in (11) will have an acceleration component dv_η/dt opposite to v_η. Given a smaller positive initial v_η, or a negative initial v_η, the particle would accelerate towards the value for v_η given in (11). This value of v_η therefore represents the η-component of a stable upgliding motion in which all the particles of the isentropic surface may join. The η-component of the stable upgliding motion approaches infinity when $2\Omega_z - \partial v_g/\partial \eta$ goes to zero. In other words, in the case of inertial indifference any finite initial v_η would increase exponentially.

Quite analogous reasoning in the case $2\Omega_z - \partial v_g/\partial \eta > 0$ and $v_x \partial v_g/\partial x + \partial v_g/\partial t < 0$ reveals the existence of stable downgliding motion in which the η-component is also given by (11).

The difference between the cases $v_x \partial v_g/\partial x + \partial v_g/\partial t = 0$ and $\gtrless 0$ is thus the following: In the former case the departures from the geostrophic wind remain of a stable oscillatory nature until the anticyclonic isentropic shear reaches the critical value of $-2\Omega_z$. In the latter cases there is a sustained stable departure from the geostrophic wind, represented by v_η, which has finite values also when $2\Omega_z - \partial v_g/\partial \eta > 0$. In addition there may be inertial perturbations superimposed on the current representing the vector sum of geostrophic motion v_g and isentropic motion v_η; such perturbations will be stable as long as $2\Omega_z - \partial v_g/\partial \eta > 0$.

The demonstration of the occurrence of anticyclonic shear in the upper atmosphere, which approaches or even surpasses the critical limit of dynamic instability, is due to recent research work at the University of Chicago. The first profile of the westerlies showing such conditions was analyzed by Palmén [23] in 1948. In the same paper it is also shown how we must treat zonal flow as curved flow (radius of curvature $r = a \operatorname{cotan} \phi$) in order to arrive at a satisfactory accuracy of an isovel profile which is to correspond to an observed meridional pressure profile. In the following discussion we shall use the model of straight baroclinic westerlies with a stationary polar front published by Palmén and Newton [24] and reprinted here as the left part of Fig. 7. It represents an isotherm-isovel profile based on an averaging of twelve eastern North American meridional profiles made during December 1946. In the right-hand part of Fig. 7 we have added a diagram of the computed quantity $2\Omega_z - \partial v_g/\partial \eta$, with η interpreted as the curvilinear isentropic coordinate (positive direction northwards). In most of the field $2\Omega_z$ is greater than $\partial v_g/\partial \eta$, indicating inertial stability; but in a narrow zone south of the maximum upper westerlies, $2\Omega_z - \partial v_g/\partial \eta$ is negative, indicating inertial instability. Furthermore, in the frontal zone below 600 mb, where $\partial v_g/\partial \eta$ has been measured along saturation isentropes, the values of $2\Omega_z - \partial v_g/\partial \eta$ indicate only a slight amount of inertial stability. We shall focus our attention first on that part of the profile.

The small positive (or in some individual cases negative) values of $2\Omega_z - \partial v_g/\partial \eta$ are located in a narrow frontal zone, while in the adjacent parts of the warm and cold air masses, $2\Omega_z - \partial v_g/\partial \eta$ is positive and far from zero. Since in (11) the component of stable upgliding or downgliding is inversely proportional to $2\Omega_z - \partial v_g/\partial \eta$, it follows that the air in the narrow frontal zone has a much greater possibility for isentropic up- or down-displacements than the air masses on either side.

The quantity $v_x \partial v_g/\partial x + \partial v_g/\partial t$, representing the numerator in the expression for v_η in (11), cannot be judged from the data of one profile alone. It will be large and positive (1) where the isobars of the horizontal pressure distribution converge, and (2) where the gradient wind increases locally with time. The first condition is fulfilled, for example, along the axis of kinematic dilatation extending eastward from a col of the pressure field. This synoptic situation is known to be frequently associated with frontogenesis and subsequent maintenance of a sharp front. The second condition, local increase of gradient wind parallel to the frontal zone, frequently occurs during frontogenesis,

but the cause of such an increase of gradient wind is not necessarily attributable to the frontal mechanism.

Whenever $v_x \partial v_g/\partial x + \partial v_g/\partial t$ has the same sign in each of the two air masses, v_η will also have the same sign in the whole field; but its maximum numerical values, as far as the lower troposphere is concerned, will be found in the frontal zone where $2\Omega_z - \partial v_g/\partial \eta$ is at a minimum.

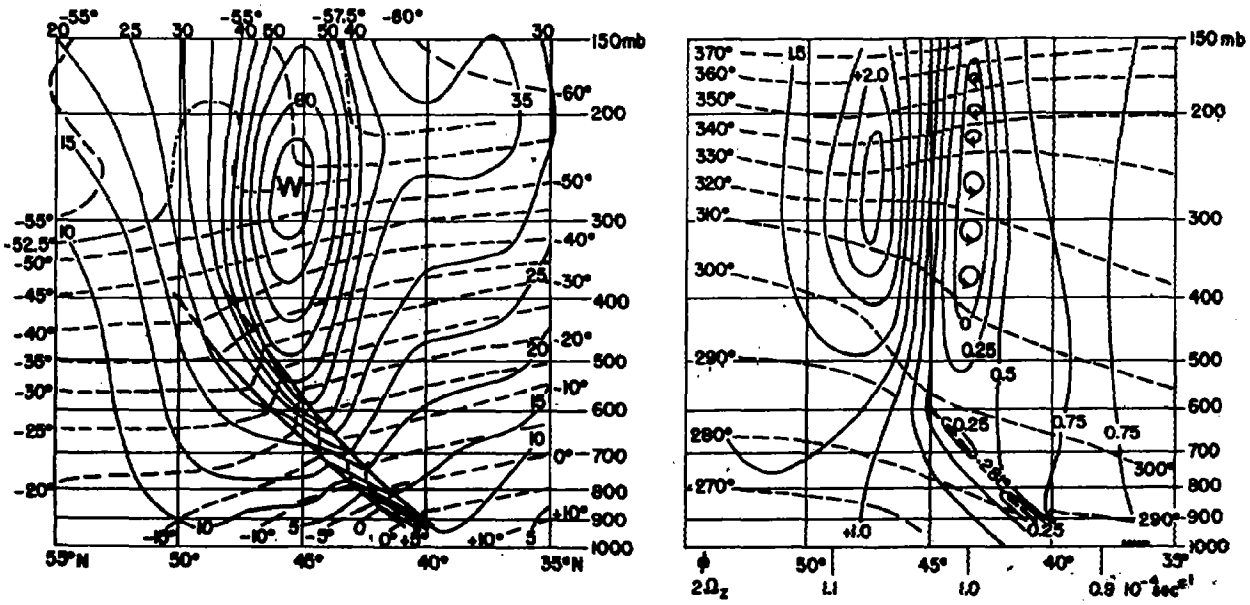

FIG. 7.—Meridional profiles through a model of straight westerlies with quasi-stationary polar front (Palmén and Newton [24]). Left: Dashed lines show isotherms (degrees centigrade), and solid lines isovels (m sec^{-1}) of zonal geostrophic wind. Right: Dashed lines show the field of dry-isentropes (degrees absolute), and the saturation-isentrope of 281° in the frontal zone. Solid lines represent the quantity $2\Omega_z - \partial v_g/\partial \eta$ in units of 10^{-4} sec^{-1}.

As shown in Fig. 7, the warm air over the lower and intermediate portion of the polar-front surface has anticyclonic isentropic shear, increasing to great values in the upper troposphere, whereas the air above the upper part of the frontal surface has cyclonic shear, likewise increasing to high values in the upper troposphere. The dividing line between anticyclonic and cyclonic shear runs almost vertically through the maximum of west-wind velocity, which in the average condition represented by Fig. 7 is located above the place where the frontal surface intersects the 500-mb level. Isentropic upgliding or downgliding as defined by equation (11) will reach larger values south of the velocity maximum than north of it. It is likely that this difference in v_η values north and south of the velocity maximum does give rise to important horizontal divergence effects because the η-component represents a nongeostrophic part of the total wind. The v_η-divergence effect in the jet-stream region should work out as shown schematically in Fig. 8. Where there is "confluence" of the winds into the western beginning of a "jet stream," equation (11) indicates a superimposed isentropic upgliding $v_\eta > 0$ and "isentropic convergence" $\partial v_\eta/\partial \eta < 0$ north of the line of maximum $|v_\eta|$. Where the wind velocity decreases along the streamlines in the "delta" of a jet stream, equation (11) indicates isentropic downgliding $v_\eta < 0$ and isentropic divergence $\partial v_\eta/\partial \eta > 0$, north of the line of maximum $|v_\eta|$. In the stratosphere the terms downgliding and upgliding must be interchanged, because of the opposite tilt of isentropic surfaces, but the statement about the isentropic divergence remains identical for stratosphere and troposphere. At the line of maximum $|v_\eta|$ values the isentropic divergence $\partial v_\eta/\partial \eta$ changes sign, as shown by the hatching in Fig. 8.

In figuring out the effect of the isentropic divergence in changing the pressure field we may think of the distribution of $\partial v_\eta/\partial \eta$ as representing in the first approximation a field of $\partial v_y/\partial y$, where v_y is the nongeostrophic

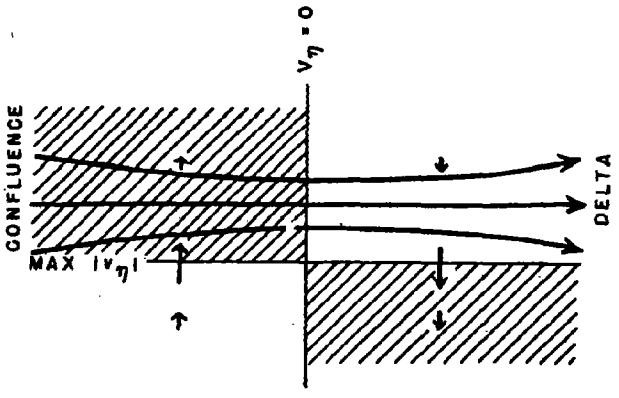

FIG. 8.—Isentropic convergence (hatched) and divergence (unhatched) in the regions of jet-stream confluence and delta.

y-component of motion. Assuming that the distribution of $\partial \rho v_y/\partial y$ can also be qualitatively represented by the hatched and unhatched areas in Fig. 8, we have in that diagram an outline of the contribution of isentropic divergence to the total horizontal divergence. The isentropic divergence, acting in the same sense through

the stratosphere and the upper half of the troposphere, may be an important effect to consider together with the divergence effects represented in Fig. 1. A cyclonic storm traveling along the jet-stream zone would come under the influence of superimposed upper mass divergence from the time when it passes the place of greatest constriction of the upper streamlines. A complete theoretical treatment of this case, which calls for a combination of the divergence effects of Fig. 1 and Fig. 8, is not available; but there seems to be considerable empirical evidence for strong cyclonic deepening under the described circumstances. Such synoptic evidence has mainly been gathered by Scherhag [30]. Scherhag points to Ryd [28, 29] as the originator of the idea that mass divergenee of importance for cyclone deepening should occur in upper delta patterns. Ryd's theoretical contributions appeared in 1923 and 1927 when there were as yet no upper-air maps.

Returning to Fig. 7, we see that complete inertial instability $\partial v_g/\partial \eta > 2\Omega_z$ may at times extend from 150 mb down towards the 500-mb surface. It may also extend over a thousand kilometers' length of current, but the width of the zone of such unstable shear is hardly more than three hundred kilometers at any one point. Inside that volume of current the geostrophic wind, with its superimposed component of isentropic upgliding or downgliding, does not represent a stable flow. However, with stable neighboring flow on either side, no very large unstable deviations from geostrophic flow will be able to develop. The most likely system of perturbations in the unstable part of the current will be helical cellular circulations, as indicated in Fig. 7. Such circulations would serve the purpose of exchanging momentum across the zone of unstable shear and thus lessen that shear. The height of each cell would have to be small, probably less than one kilometer, so that the solenoid field set up by the cellular circulation should not grow strong enough to reverse the initial circulation. An indirect indication of the existence of the helical cellular circulations is seen in the observed "multiple tropopauses," each one probably representing a cell wall between superjacent circulation rolls. According to Palmén [22], these multiple tropopauses are quasi-isentropic as would be expected if they are formed as circulation-cell boundaries.

SYNOPTIC EXAMPLE OF AN EXTRATROPICAL CYCLONE

The weather situation over North America during November 7–10, 1948, has been selected to illustrate the principles of this article. A large occluded cyclone which was located over the Hudson Bay region during this period can serve as a model of the most frequent structure of old cyclones, while over the central United States the atmosphere displays all the successive stages of frontogenesis and the early life history of a growing frontal wave cyclone. Our description will begin with the evolution of the long-wave background pattern of the upper layers, represented by a set of 300-mb maps, then the advective frontogenesis in the lower troposphere will be illustrated by a sequence of ground-level and 850-mb maps as well as selected profiles, and finally the three-dimensional structure of the frontal wave cyclone will be shown by a synoptic set of maps from the ground to 300 mb.

Synoptic Evolution of the Upper Layers. The six 300-mb maps at 12-hr intervals in Fig. 9 all show the semipermanent Hudson Bay cyclone. Through the whole troposphere this cyclone is a cold-core vortex and therefore shows up as a deep center on the 300-mb maps. Equally permanent is the crest of high pressure extending northwards from a warm anticyclone over the eastern North Pacific. Both the Hudson Bay low and the eastern Pacific high are typical features of the general circulation but they have more than average strength during November 7–10. The westerly current meandering through between them is quite strong over a narrow zone, while the pressure gradients in the high and the low are quite weak. The trough located over the western United States on November 7 moves slowly to the central states and deepens gradually from November 7 to November 9. This upper-air process plays an important role in the formation of the frontal cyclone which takes place under the pre-trough southwesterly current (without producing any separate low-pressure center at 300 mb).

The deepening of the upper trough may be caused in two ways (see equation (1)): either through a sinking component of motion at the 300-mb level, or through horizontal mass divergence in the column above 300 mb. In the former case the temperature in the trough at 300 mb ought to be rising with time. This is not borne out by the observations during November 7–9, so that we are left with the horizontal mass divergence as the probable cause of the deepening of the trough. The mass divergence must be operated through the feeding of air into the trough with such a high velocity that the Coriolis force and centrifugal force overcompensate the initial pressure gradient. The mechanism for producing such a strong jet in the northerly current behind the trough must be sought on the anticyclonic bend to the west.

The maximum curvature of the 28,400-ft contour of the 300-mb surface is represented on the November 7th map by an arc of a circle with radius r_i. At the same place in western Canada the maximum possible curvature of a steady-state anticyclonic current, flowing under the influence of the observed pressure-gradient force, is represented by another arc of a circle with radius r_{min}.[3] The curvature analysis on the 300-mb

3. The value of r_{min} is obtained from the equation of anticyclonic circular motion

$$-v^2/r = -2\Omega_z v - \partial\Phi/\partial r = -2\Omega_z(v - v_g), \qquad (12)$$

in which Φ stands for the geopotential in the pressure topography, r and v are positive, $-\partial\Phi/\partial r$ is the outward-directed pressure gradient, $-2\Omega_z v$ is the inward-directed Coriolis force, and $-v^2/r$ is the centripetal acceleration. When equation (12) is applied to a selected point on the map, Ω_z and $\partial\Phi/\partial r$ are

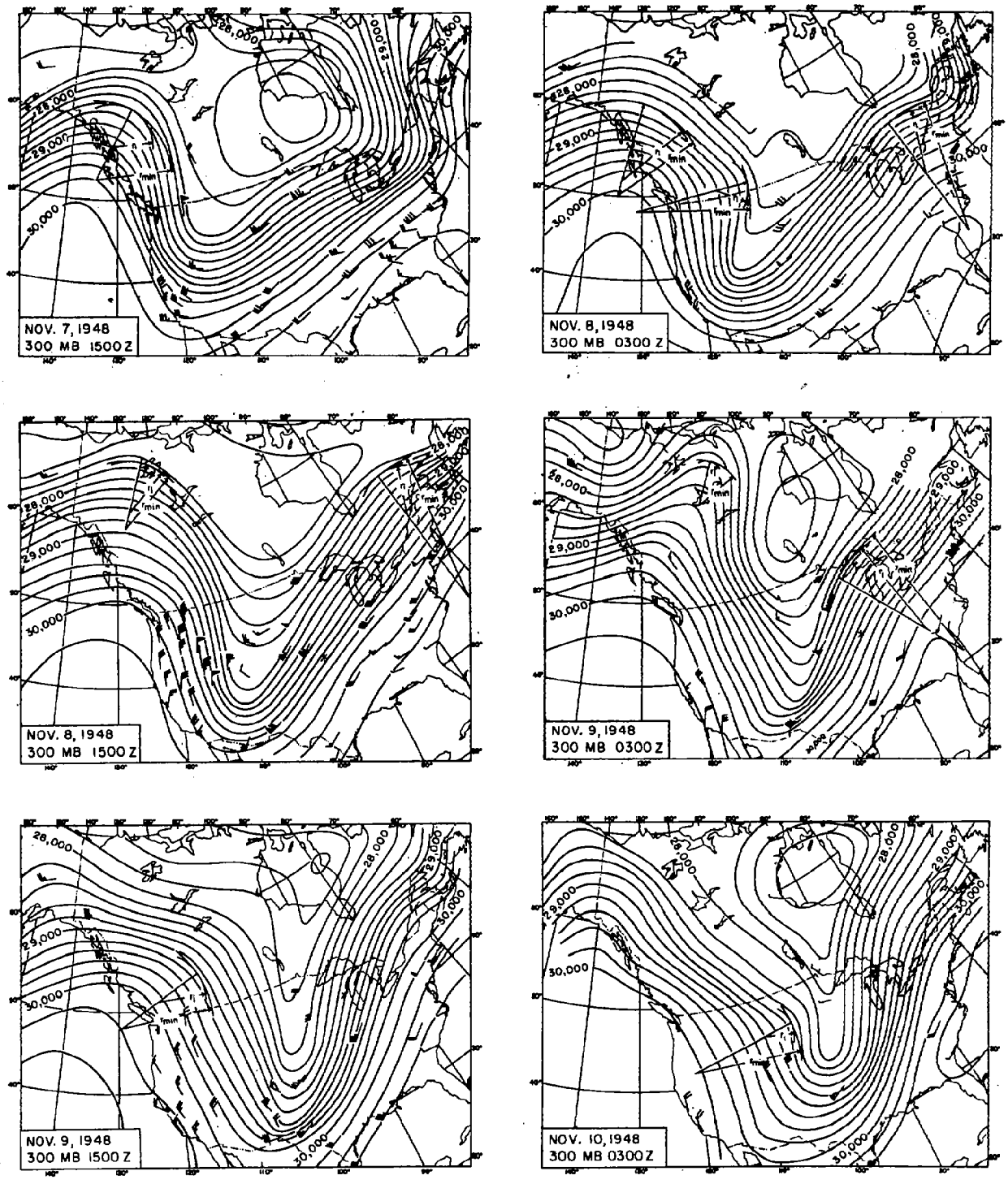

FIG. 9.—Twelve-hourly sequence of 300-mb maps during November 7–10, 1948 (r_i = radius of isobaric curvature, $r_{min} = -\frac{\partial \Phi}{\partial \tau}/\Omega_s^2 = 2v_g/\Omega_s$). Asterisk marks position of apex of frontal wave on sea-level map. Half barb 5 m sec^{-1}, full barb 10 m sec^{-1}, triangular barb 50 m sec^{-1}.

anticyclonic bend over western Canada on November 7 and the following days shows that instances of $r_i < r_{min}$ are quite frequent, in other words, that with the given pressure gradient and contour curvature the paths of particles often cannot have as small a radius of curvature as that of the isobaric contours. If that applies to a quasi-stationary pressure ridge like the orographic one over the Canadian Rockies, where the radius r_s of streamline curvature is equal to the radius r of path curvature, the air would have to cross the isobars towards low pressure while making the anticyclonic turn. This must imply a forward acceleration of the particle leading up to maximum speed at the end of the anticyclonic sweep. If such fast-moving air is fed directly into a pressure trough downstream, in which the pressure gradients were adapted to smaller wind speeds, an intensification of the trough should follow. The deepening of the large pressure trough over western and central United States during November 7–9, 1948, should probably be interpreted this way. Measured winds are unfortunately not available for a complete check of these ideas. The only part of the phenomenon that can be well demonstrated is the general occurrence of wind components towards high pressure, resulting from the supergeostrophic velocity of the air that is leaving the anticyclonic bend (see winds over the western United States on the 300-mb map of November 8, 1500Z).

The flow around the quasi-stationary anticyclonic bend over western Canada cannot be a steady-state one, although the major features of that part of the map do remain unchanged. The 300-mb maps show how one moving wave perturbation after the other appears on top of the large stationary crest of high pressure in the west. The first of these traveled about 1500 km during twelve hours (35 m sec^{-1}) and is found on the second map with its wave crest in the northerly current at the Canadian-United States border. The 300-mb contour curvature at that time and place defines an r_i which is much smaller than r_{min}.

The radii of curvature of streamlines, r_s, and of air trajectories, r, in a moving sinusoidal wave, are related to each other by the formula

$$r_s = r\frac{v - c}{v}, \tag{16}$$

where c is the speed of the wave. No measured wind velocities are available at 300 mb in western Canada during the days under consideration. Theoretical estimates of v must lie between v_g and $2v_g$, and are most likely closer to the lower than the upper limit, as will be shown later. Assuming tentatively for the moving pressure crest at the Canadian–United States border on November 8, 0300Z, $v = 1.1v_g = 49$ m sec^{-1}, we would have from (13)

$$r = \frac{49^2}{1.08 \times 10^{-4}(49 - 44.5)} = 4900 \text{ km},$$

and would arrive at the following estimate of r_s:

$$r_s = 49 \times 10^5 \frac{49 - 35}{49} \text{ m} = 1400 \text{ km},$$

which is much longer than the measured radius of contours $r_i = 440$ km. These estimates and measurements are of course subject to great errors, but even so, the conclusion seems to be that also on the moving pressure crests the streamlines will fail to adapt to the strong curvature of the isobars. It then also follows that the moving pressure crests at the 300-mb level are preceded by a velocity maximum. When the air from that velocity maximum enters the slow-moving low-pressure trough, a pulse of deepening by centrifugal action would result. The rapidly moving upper wave cannot be seen to continue its propagation on the front side of the deep slow-moving trough. Hence all its wave energy must have been absorbed in the large trough.

With the above estimate of $v = 49$ m sec^{-1} and $r_s = 1400$ km, the anticyclonic vorticity due to curvature $-v/r_s$ amounts to -3.5×10^{-5} sec^{-1}. This is numerically much less than $2\Omega \sin 50° = 1.1 \times 10^{-4}$ sec^{-1}, so it does not seem likely that the complete anticyclonic vorticity $-v/r_s - \partial v/\partial n$ reaches the critical value of $-2\Omega_s$ anywhere in the rapid wave at 300 mb. The described manifestation of instability through cross-isobaric flow on the anticyclonic bend thus takes place independently of the fulfillment of the criterion $-v/r_s - \partial v/\partial n + 2\Omega_s < 0$.

On November 8, 1500Z, when the most unstable part of the anticyclonic flow was found far north (again marked by $r_i < r_{min}$), a growing crest and a downwind, deepening trough formed simultaneously. When that perturbation caught up with the slow-moving trough ahead, another deepening occurred (see November 9, 1500Z), this time in the north-central United States while the southern end of the trough was losing depth.

These fast-moving unstable waves on the 300-mb maps are, of course, at times connected with disturbances in the lower atmosphere. The first of the upper waves was formed on November 7, 1500Z, as an occluded front was approaching from the west; it is likely that the excessive anticyclonic curvature resulted from a superposition of the upper wave crest (associated with the occluded cyclone) upon the semipermanent anticyclonic bend produced orographically by the northern Rocky Mountains. Once formed, the unstable

---

constants. Solving (12) for

$$r = \frac{v^2}{2\Omega_s v + \partial\Phi/\partial r} = \frac{v^2}{2\Omega_s(v - v_g)}, \tag{13}$$

and seeking the value of v for which r is a minimum, we obtain

$$v = \frac{-\frac{\partial\Phi}{\partial r}}{\Omega_s} = 2v_g. \tag{14}$$

The corresponding values of r_{min} and v are thus

$$r_{min} = -\frac{\frac{\partial\Phi}{\partial r}}{\Omega_s^2} = \frac{2v_g}{\Omega_s}, \qquad v = 2v_g. \tag{15}$$

upper wave separates from the frontal disturbance by virtue of its superior speed (35 m sec^{-1}). The second unstable upper wave had no clear connection with any frontal disturbance.

During the selected period, the flow of air east of the big slow-moving trough turned gradually from west-southwest towards south-southwest while increasing a little in strength. On November 8, 1500Z, after the cold trough of the Hudson Bay cyclone had moved off to the northeast, the upper current over the eastern half of the United States and Canada became almost straight. On November 9, 0300Z, when the growing frontal cyclone (marked by an asterisk on the 300-mb maps) began to exert influence high up, the upper current became slightly S-shaped. The newly formed upper wave moved along with the cyclone center below at a speed of only 9 m sec^{-1}. The best estimate of the wind speed on the anticyclonic bend is probably 80 m sec^{-1} (see below) and hence $r_s = r(80 - 9)/80 = 0.9r$. Even with $r = r_{min} = 1950$ km, r_s would be 0.9×1950 km = 1760 km, which is greater than the measured $r_i = 1350$ km. The streamlines will consequently not be able to adapt to pressure contours around the anticyclonic bend.

The tentative assumption of $r = r_{min}$ given above is really predicated on the further assumption that the wind maintains a speed of $2v_g$ around the anticyclonic bend. We can in this case show convincingly that the wind does not reach such a speed and therefore that the air trajectory must have a radius of curvature considerably longer than r_{min}.

The geostrophic wind in the strongest part of the straight southwesterly current on November 8, 1500Z amounted to about 70 m sec^{-1}, and on the chart for November 9, 0300Z a measurement of the geostrophic wind in the Great Lakes region gives nearly the same value. Even at the geostrophic speed of 70 m sec^{-1}, which gives a speed of $70 - 9 = 61$ m sec^{-1} relative to the wave, it would take only 4½ hours for each air parcel to cover the 1000-km distance along which there is anticyclonic curvature. Suppose a particle passes the inflection point at 70 m sec^{-1} and from then on experiences a forward tangential acceleration $(dv/dt)_t = 2\Omega_n v_r$ on the anticyclonic bend. If v_r, the wind component directed outward normal to the isobars, reaches the high average value of 10 m sec^{-1} on the anticyclonic bend, the speed of the particles would increase at a rate of 10 m sec^{-1} per three hours, and at most by 15 m sec^{-1} during the whole travel from inflection point to inflection point. This increase in speed would thus go only one-fifth of the way from v_g to $2v_g$. This reasoning justifies the earlier assumption of the moderately supergeostrophic wind of $70 + 10 = 80$ m sec^{-1} on the middle of the anticyclonic bend.

Another effect of the transisobaric wind component on the anticyclonic bend is also worth considering. A flow component across anticyclonic contours towards low pressure is usually synonymous with horizontal divergence of mass, and offers in that way a contribution to pressure fall (see equation (1)). The basic pattern in Fig. 1 of horizontal divergence in westerly waves would thus, in the levels of strongest westerlies, show the divergence extending forward beyond the ridge of highest pressure. The implications of this divergence on the pressure ridges of the upper atmosphere for the storm development in the lower atmosphere will be considered on p. 597.

Frontogenesis. Figure 10 illustrates three stages of frontogenesis, 24 hours apart, represented by simultaneous sea-level and 850-mb maps. At the first map time the Hudson Bay cyclone is also shown. Its thermal structure is that of an old cyclone with the occluded front beginning to wrap around the center. The upper warm tongue, extending east and north of the Hudson Bay center from the warm-air reservoir over the Atlantic, is shown clearly in the 850-mb isotherms. The pressure trough pointing southwards from the Hudson Bay cyclone is not of frontal nature, as can be seen from the weak temperature gradient at 850 mb in that region. The same nonfrontal trough continues up to the 300-mb level (Fig. 9), where its orientation approaches northwest-southeast, and in those upper layers it actually extends out over the Atlantic, producing a bend in the warm sector current. Such troughs always move more slowly than the air, and it is kinematically impossible for fronts to develop in them.

Historical continuity made it obvious that the cold front from the Hudson Bay cyclone had reached Florida by November 7, 1500Z, but the 850-mb map shows how the cold air, after arriving over the Gulf States, must have subsided and thereby effaced most of the frontal temperature contrast. The bundle of isotherms running along the northern part of the cold front bends westward over the Carolinas and northern Georgia and there marks the intersection of the 850-mb map with the tilting surface of subsidence. The 850-mb winds in that region blow across the isotherm bundle from cold to warm, but fail to produce any local fall in temperature because of the simultaneous sinking. The deviations from geostrophic flow are quite striking in that sinking air mass. While descending from the levels of strong west winds the air particles must be retarded and, in order to do so, they must move with a component towards high pressure, as shown on the 850-mb map of November 7, 1500Z. The same type of geostrophic departure is found on that day over the southeastern United States all the way up to 300 mb (Fig. 9). On the following day (November 8), the geostrophic departures characteristic of the front side of moving anticyclones can be seen on the 850-mb map over New England. In the rear of the moving anticyclone the opposite geostrophic deviation is observed. In that part the air is ascending and accelerating and must have a horizontal component towards low pressure. This phenomenon is actually part of the process of frontogenesis over the central United States which will be considered next.

Frontogenesis by horizontal advection operates when a field of deformation is maintained in a baroclinic air mass. Optimum efficiency in this process is achieved when the axis of dilatation of the field of deformation coincides with the direction of the isotherms. The

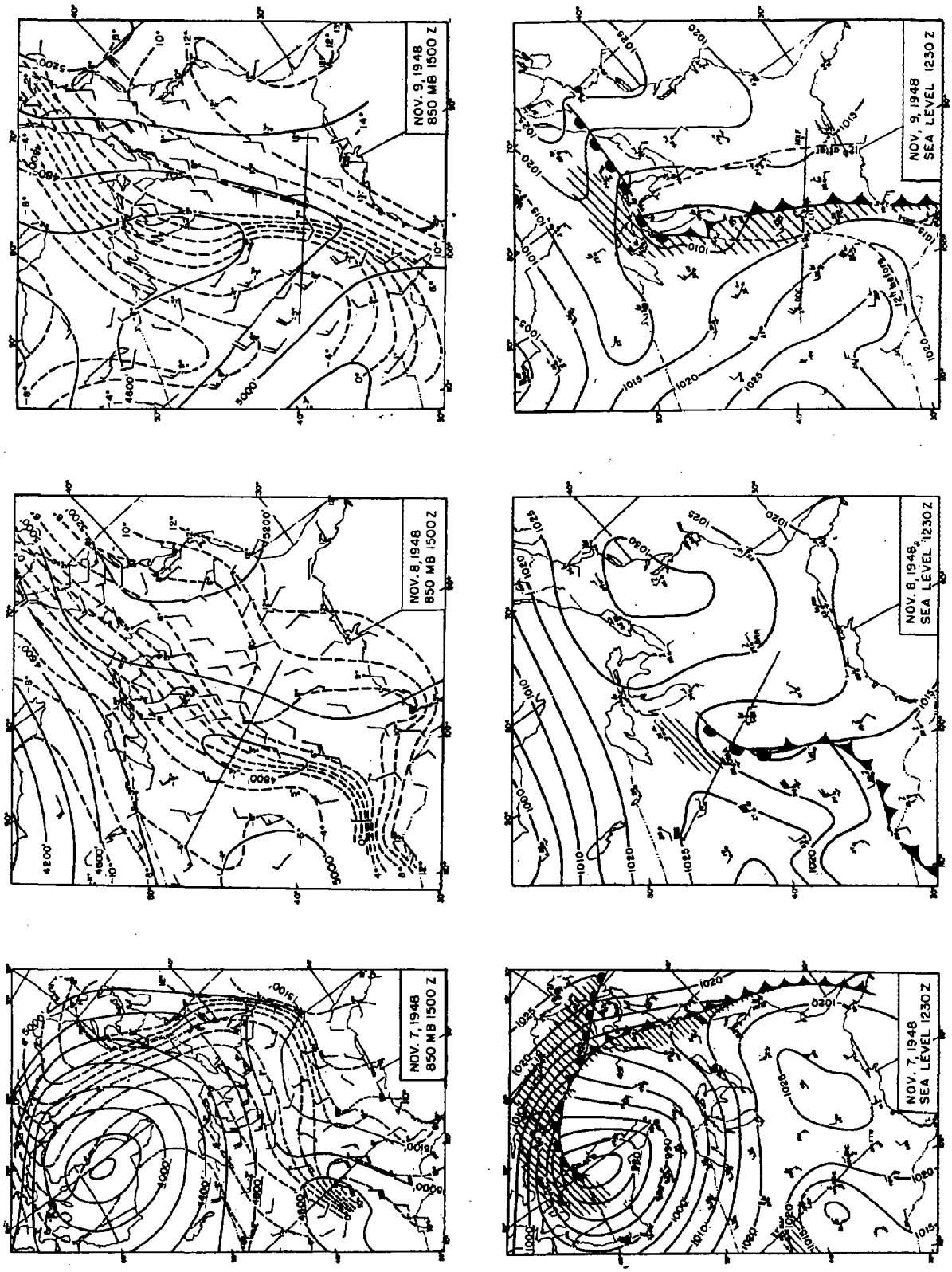

FIG. 10.—Twenty-four-hourly sequence of sea-level and 850-mb maps, showing advective frontogenesis and incipient cyclogenesis. Upper winds: Half barb 5 m sec^{-1}, full barb 10 m sec^{-1}.

streamlines in the col over the central United States on November 7, 1500Z, fulfill that condition fairly well. The mentioned geostrophic departure towards low pressure on the warm side of the col also favors the transportation of the isotherms towards the axis of dilatation. As a result of these processes a surface front has formed on November 8, 1500Z, over the region previously occupied by the col, while frontogenesis is in progress over the Great Lakes region where the col has now arrived. A frontal wave has already formed over the state of Missouri and is represented in the pressure field by a small elongated low. During the following twenty-four hours the new cyclone deepens and moves along the front northeastward. A new field of deformation is active on November 9 along the cold front of that cyclone and helps maintain the frontal temperature contrast.

The described frontogenetical development near the ground conforms with the advective rules set forth by Bergeron [1] and Petterssen [25]. We shall here add a study of the dynamical conditions for isentropic upgliding in the free atmosphere, which is an important part of the process of frontogenesis.

The rate of frontogenesis near the ground is increased considerably if the air of the lower part of the frontal zone is removed by upgliding. The dynamical possibilities for that process are considered in Fig. 11, which contains a profile across the zone of frontogenesis during its early stage on November 7, 1500Z. At that time no clear-cut front was yet discernible on the surface map, but on the 850-mb map there is great crowding of isotherms between the cold air over North Platte and the foehn air over Dodge City. The foehn on the warm side of the col gives the frontogenesis a good start in the layers below the level of the continental divide, but the process also takes place higher up, as shown by the isothermalcy between 600 and 560 mb at Rapid City.

The thermodynamics of upgliding in the sloping frontal zone can be tested through an inspection of the 293° dry-isentrope which has been inserted in Fig. 11. It shows that a particle could be brought dry-adiabatically along the profile from near the ground in Oklahoma to the tropopause at 350 mb over Montana without being subject to stabilizing gravity effects. If we take into account that condensation would begin in such a particle at 700 mb, the ascent from there on would follow the saturation isentrope of 282°, which climbs more steeply than the dry-isentrope and likewise reaches the tropopause. Actually no single particle undergoes such far-reaching isentropic displacements inside the profile; but the isentropes can still be used as indicators of the direction of the component of stable upgliding (see p. 585), which the particles may have in addition to their much stronger geostrophic component of motion normal to the profile.

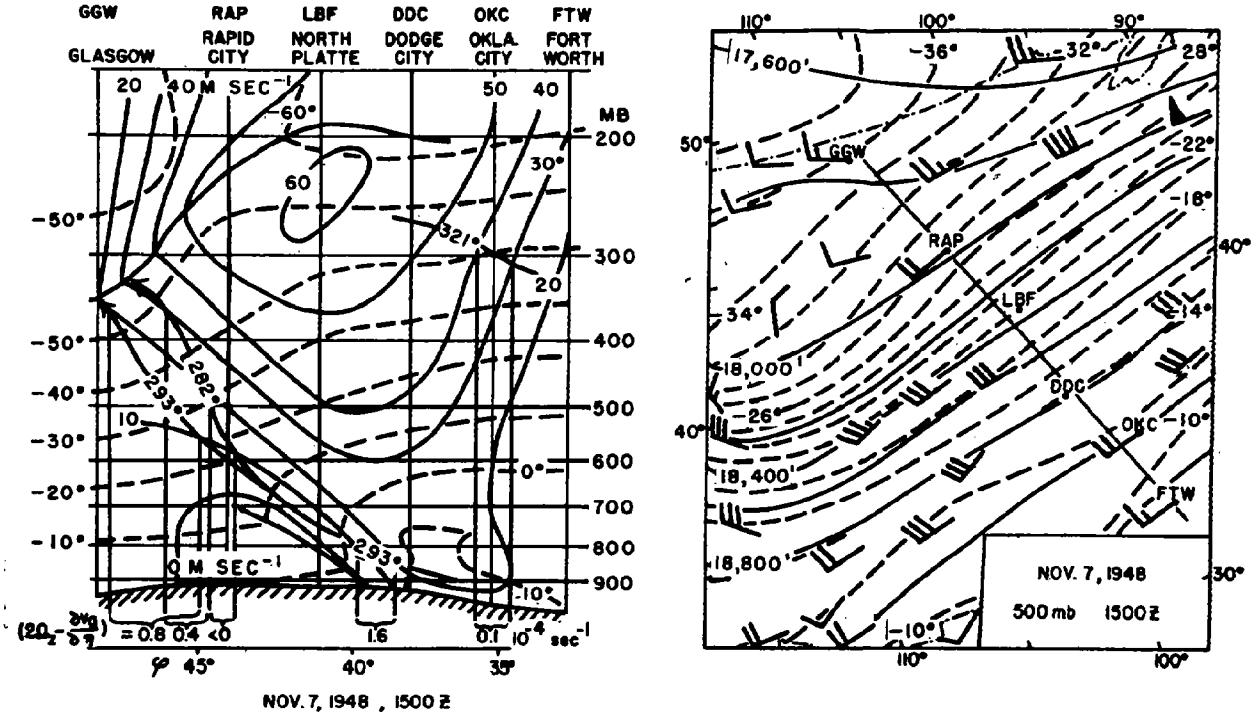

FIG. 11.—Profile of early frontogenesis, November 7, 1948, 1500Z, and part of the 500-mb map for the same time. Sample evaluations of $2\Omega_z - \partial v_g/\partial \eta$ below diagram. Upper winds: Half barb 5 m sec^{-1}, full barb 10 m sec^{-1}, triangular barb 50 m sec^{-1}.

A study of the values of the isentropic upgliding (equation (11)),

$$v_\eta = \frac{v_x \dfrac{\partial v_g}{\partial x} + \dfrac{\partial v_g}{\partial t}}{2\Omega_z - \dfrac{\partial v_g}{\partial \eta}},$$

along the different sections of the inserted isentropes, will reveal the dynamical possibilities for frontogenesis.

The denominator in the expression above can be determined uniquely from the data contained in the profile, whereas the numerator depends on derivatives of the geostrophic wind normal to the profile and derivatives in time. Let us consider the denominator first.

Along the lower part of the 293° isentrope the geostrophic shear $\partial v_g/\partial \eta$ is negative, and hence $2\Omega_z - \partial v_g/\partial \eta$ is large. Between the points of intersection of the 293° isentrope with the isovels of 20 m sec^{-1} and 10 m sec^{-1} the value of $2\Omega_z - \partial v_g/\partial \eta$ can be computed to be 1.6×10^{-4} sec^{-1}, as indicated at the bottom of the profile. Farther up along the 293° isentrope, $\partial v_g/\partial \eta$ changes sign and $2\Omega_z - \partial v_g/\partial \eta$ decreases despite the northward increase of $2\Omega_z$. In the baroclinic field between Rapid City and Glasgow $2\Omega_z - \partial v_g/\partial \eta$ has decreased to 0.8×10^{-4} sec^{-1}. Still smaller values are found along the 282° saturation isentrope, and a negative $2\Omega_z - \partial v_g/\partial \eta$ results in the section near Rapid City. The latter value indicates dynamic instability or, in other words, the condition of upgliding without dynamic brake action. Actually only small volumes of saturated air (altostratus and cirrus) occur in the region under consideration during the early stage of frontogenesis, and friction of such air against the dry environment probably exerts enough of a brake action to preclude violent developments. The dry-adiabatic upgliding thus still applies to the greater part of the baroclinic upper-tropospheric air.

The numerator in the expression for v_η can be judged from an inspection of the 500-mb map (in Fig. 11). If $v_x \partial v_g/\partial x$ is measured on the map just north of Rapid City, it amounts to $20 \times 2.6 \times 10^{-5}$ m sec^{-2} $= 5.2 \times 10^{-4}$ m sec^{-2}. The large value of the term comes from the convergence of the 500-mb contours and that feature, in turn, is inherent in the structure of the large pressure trough to the west with its central area of weak pressure gradient bordering on strong pressure gradients to the south. The large value of $\partial v_g/\partial x$ is, of course, also corroborated by measured wind velocities, which increase from 10 m sec^{-1} to 50 m sec^{-1} along the streamline from northern Wyoming to Green Bay, Wisconsin. In addition, the 300-mb map (Fig. 9) shows the same convergence of contours a little farther north.

An evaluation of v_η at the 500-mb level just north of Rapid City gives

$$v_\eta = \frac{5.2 \times 10^{-4}}{0.8 \times 10^{-4}} = 6.5 \text{ m sec}^{-1}.$$

Here $\partial v_g/\partial t$ has been neglected as insignificant in comparison with $v_x \partial v_g/\partial x$. The corresponding v_x would be about one-hundredth of v_η, hence 6.5 cm sec^{-1}. Corresponding determinations of v_η lower down on the frontal slope result in smaller values, and consequently $\partial v_\eta/\partial \eta$ is positive. With $\partial v_\eta/\partial \eta$ and $\partial v_x/\partial x$ both positive in the frontal zone, there is stretching in both the η-direction and the x-direction, so that frontogenesis progresses under optimum conditions.

In the upper troposphere south of the maximum westerlies $\partial v_g/\partial \eta$ assumes large values approaching those of $2\Omega_z$. In Fig. 11, $2\Omega_z - \partial v_g/\partial \eta$ measured at 300 mb over Oklahoma City is only 0.1×10^{-4} sec^{-1}. However, $v_x \partial v_g/\partial x + \partial v_g/\partial t$ is also small at that place (see Fig. 9) so that no great v_η-component results. Farther east near the Atlantic, where the anticyclonic isentropic shear is equally great and $v_x \partial v_g/\partial x$ has a large negative value, v_η is observed to have a large negative value (directed towards high pressure) at all reporting upper-wind stations. This is an example of the systematic nongeostrophic wind components at the "delta" of an upper jet stream derived in Fig. 8. The horizontal convergence resulting in the southern half of the delta is instrumental in providing the pressure rise ahead of the moving high in the southeastern United States (Fig. 10).

Figure 12 shows a profile through the zone of frontogenesis twenty-four hours later. The frontal slope has become steeper ($\frac{1}{50}$ in the lowest portion) and the frontal shear $-\partial v_x/\partial y$ is now characterized by a sharp 180° wind shift. Negative v_g values (northeast wind) stronger than 10 m sec^{-1} now occur in the lower part of the cold wedge near the front. Applying the v_η-formula to particles in the northeast current, we find conditions set for isentropic downgliding because the numerator $v_x \partial v_g/\partial x + \partial v_g/\partial t$ is now negative. A numerical estimate of the downgliding along the 281° isentrope near the cold edge of the frontal zone at 850 mb follows:

$$v_\eta = \frac{v_x \dfrac{\partial v_g}{\partial x} + \dfrac{\partial v_g}{\partial t}}{2\Omega_z - \dfrac{\partial v_g}{\partial \eta}} = \frac{-10 \times 1.4 \times 10^{-5} - 10^{-4}}{0.96 \times 10^{-4} - 0.1 \times 10^{-4}} = -2.8 \text{ m sec}^{-1}.$$

The resulting dry-isentropic descent traverses the frontal zone with a component from the cold to the warm side. This nongeostrophic component towards the frontal trough, together with the frictional flow component in the same direction, accounts for the subgeostrophic displacement of warm fronts in general. In some cases the nongeostrophic component normal to the front may permit the cold wedge to advance against a moderate geostrophic component from warm to cold.

In the upper part of the frontal zone, isentropic upgliding continues on November 8 just as on November 7, as can be seen from the convergence of contours between Omaha and Bismarck on the 500-mb map (Fig. 12). The same contour convergence is found right over Omaha on the 700-mb map (not reproduced). In the profile the 284° saturation isentrope approximately follows the warm edge of the frontal zone; $\partial v_g/\partial \eta$ measured along that isentrope gives values greater than $2\Omega_z$ from the condensation level up to 700 mb. This lower portion of the frontal zone is thus dynamically unstable; while higher up, where the 284° isentrope turns parallel to the v_g-isovels, finite speeds of upgliding can be determined. An estimate of the upgliding on the saturation isentrope of 284° at the 500-mb level gives

$$v_\eta = \frac{23 \times 1.4 \times 10^{-5}}{(1.0 - 0.1) \times 10^{-4}} = 3.6 \text{ m sec}^{-1}.$$

Exploring the whole frontal zone for nongeostrophic isentropic motion, we find the conditions for downgliding limited upwards by the zero isovel, while upgliding begins above that line. Moreover, we find that the dry-isentropes indicate a downgliding with a horizontal component across the front from cold to warm, while the upgliding along saturation isentropes remains almost parallel to the frontal slope. The frontal profile therefore must begin to bulge forward from cold to warm in the lower layers while remaining rather unchanged higher up. That is what happens when the apex of the frontal wave goes by, as will be discussed in connection with the maps in Fig. 14.

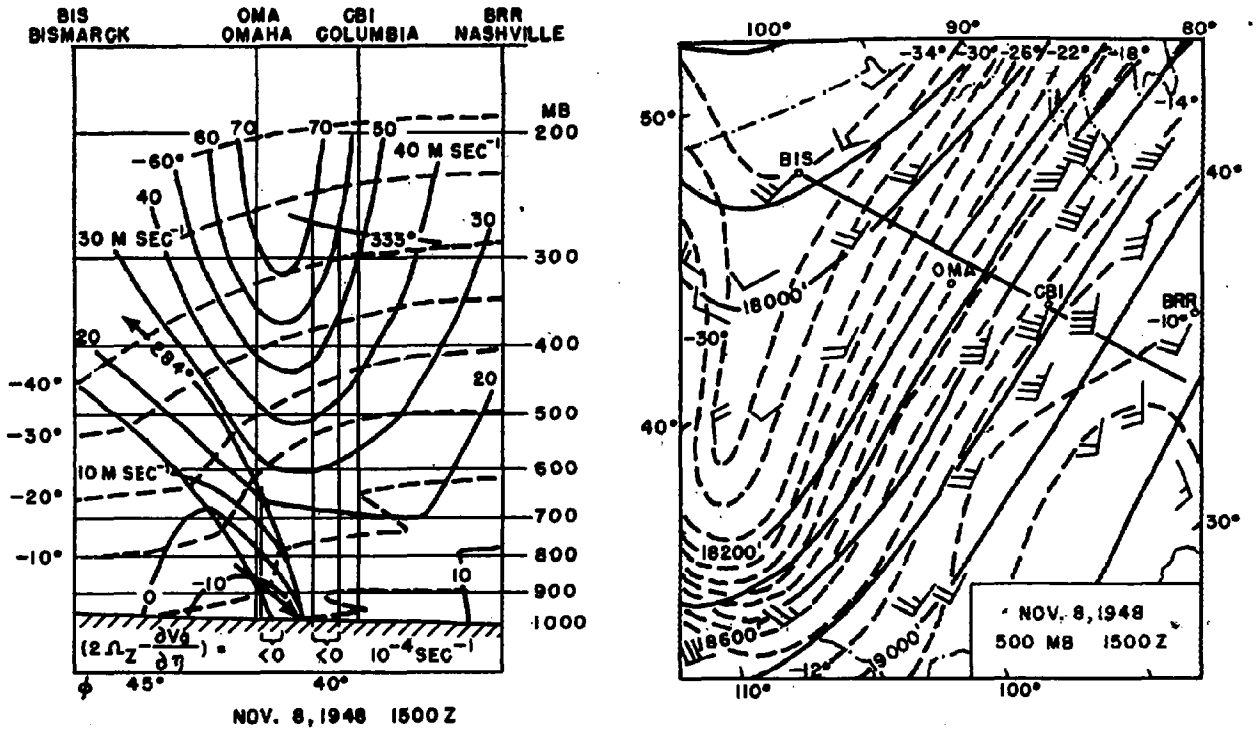

FIG. 12.—Profile of the warm front of the incipient wave on November 8, 1948, 1500Z, and part of the 500-mb map for the same time. Sample evaluations of $2\Omega_z - \partial v_g/\partial\eta$ below diagram. Upper winds: Half barb 5 m sec^{-1}, full barb 10 m sec^{-1}.

The anticyclonic shear south of the westwind maximum has grown to the state of dynamic instability as shown in Fig. 12 by means of the differentiation of v_g along the 333° isentrope. Shears rather close to the instability limit also extend down to the 500-mb level and make possible the rather large and systematic wind component towards low pressure observed on the 500-mb map southeast of the jet stream.

Figure 13 shows a profile across the cold front from Dodge City (Kansas) to Maxwell Field (Alabama) on November 9, 1500Z. The corresponding sea-level and 850-mb maps are to be found in Fig. 10. The profile shows that strong horizontal temperature gradients have formed all the way to the top of the diagram. The frontogenetical process by horizontal advection has actually been operating through the whole troposphere (in Fig. 14 the resulting frontal zone shows up well even at the 300-mb level). The inclination of the frontal zone is about $\frac{1}{50}$ in the upper portion, and it is quasi-vertical near the ground, while an intermediate portion around 700–800 mb tilts only by $\frac{1}{130}$. The general shape of the profile can be understood as the result of the bulging forward of the lower portion of the cold wedge after the passage of the frontal wave apex. The

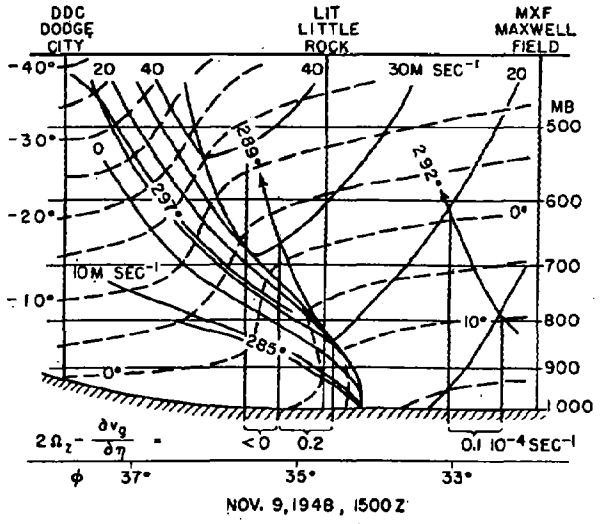

FIG. 13.—Profile of the cold front on November 9, 1948, 1500Z. Sample evaluations of $2\Omega_z - \partial v_g/\partial\eta$ below diagram.

nongeostrophic downgliding responsible for that process was found to be dynamically justified from the study of the frontal profile 24 hours earlier, $v_x \partial v_g/\partial x +$

$\partial v_g/\partial t$ being negative in the lower portion of the cold wedge. The sea-level map for November 9, 1500Z (Fig. 10) shows a positive $\partial v_g/\partial x$ along the whole cold front (the geostrophic wind component parallel to the front in the cold air is increasingly negative as we pass towards the negative x-direction), but the actual wind component v_x, parallel to the front, is about zero in the forward part of the cold wedge; $\partial v_g/\partial t$ also is small. Hence it follows that the isentropic downgliding v_η should be insignificant except where $2\Omega_z - \partial v_g/\partial \eta$ is zero or negative. The profile in Fig. 13 shows an almost perfect parallelism of v_g-isovels and dry-isentropes in the cold wedge, so that $\partial v_g/\partial \eta = 0$. Therefore, no dynamic instability occurs inside the cold air, not even in the upper part where the frontal zone is quite steep. The only place for dynamic instability to occur inside the cold air is right at the quasi-vertical part of the frontal surface near the ground, where a real temperature discontinuity exists. However, the air volume involved is too small to appear on a profile of the scale used in Fig. 13. The release of the dynamic instability at the cold front is responsible for maintaining the downdraft, which is always observed in a strip of a few kilometers' width following the frontal passage. This cold-air downdraft is instrumental in giving the cold front a greater speed of displacement than would have been indicated by the geostrophic wind determined from the sea-level pressure distribution. In Fig. 10 the computed twelve-hour geostrophic displacement of the cold front is represented by a short arrow of 80-km length, while at the same place the preceding twelve-hour displacement was 210 km and the subsequent one 460 km. The geostrophic wind component normal to the front computed from the 850-mb map is large enough to account for the frontal displacement, and we must assume that air from this level enters the frontal downdraft and carries westerly momentum to the surface layer. In the layers above 850 mb the cold-air current is cyclonically curved and hence subgeostrophic. With increasing height, the wind in the frontal zone also becomes more and more parallel to the frontal boundary, so that the frontal displacement is less there than at the ground.

The prefrontal air in the profile in Fig. 13 has a lapse rate slightly less than the saturation adiabatic, but with the existing horizontal temperature gradient a saturation-adiabatic ascent is possible at the rather steep angle of $\frac{1}{50}$, as shown by the sample saturation isentropes of 289° and 292°. The measured values of $2\Omega_z - \partial v_g/\partial \eta$ show a close approach to dynamic indifference and even some dynamic instability. A saturation-isentropic upgliding is in order at 850 mb, as can be seen from the convergence of contours ($v_x \partial v_g/\partial x > 0$) in the warm current intersected by the profile (Fig. 10). The same is true for the 700-mb map (not reproduced) but not for the 500-mb and 300-mb maps (Fig. 9). The frontal upgliding should therefore be confined to the layers under 500 mb. This is also verified by the Little Rock sounding, which goes up through the cold-front rain but shows a 35 per cent relative humidity at 500 mb. Thunderheads growing up from the cloud mass of the cold front would, of course, go well beyond 500 mb, but such phenomena of "vertical instability" were not reported in the case under consideration. Intermittent, light prefrontal rain, which was reported as far as 300 km ahead of the cold front, can be accounted for quite well by the saturation-isentropic upgliding. In the warm season such upgliding in the tropical air current may be sufficient to trigger thunderstorm formation, which in turn may develop prefrontal squall lines.

Structure of the Maturing Frontal Cyclone. Figure 14 presents the sea-level, 700-mb, 500-mb, and 300-mb maps for November 10, 0300Z, depicting the structure of the maturing frontal cyclone. The amplitude of the frontal wave on the surface map has now increased considerably, and the cold air from the rear begins to encircle the cyclone center. It is clearly seen how this occlusion process has had its inception only at the ground, while the isotherm patterns of the upper maps still indicate an open wave of small amplitude. This shows that while the wave travels along the front the frontal slope increases to a maximum at the wave apex. At that point the smooth wave "breaks" and a relatively shallow cold outbreak fans out along the ground. The mechanism of this breaking of the smooth wave probably lies in the dynamic instability of the lower part of the frontal zone, described in its stage of inception in Fig. 12 and continuing in the form of the frontal downdraft in Fig. 13. During the process, the cold front part near the cyclone center undergoes frontolysis through cold-air downgliding. This is always noticeable in the surface-map analysis, and, on November 10, 0300Z, it also shows up in a weakening of the frontal temperature gradient on the 700-mb map. Farther south, where the cold front passes through the frontogenetical field of deformation, the frontal temperature gradient remains rather strong. The strongest frontal temperature gradient, however, is found at the 500-mb level where the breaking of the frontal wave has not yet started. The 300-mb map also shows fairly strong temperature gradients across the pressure trough, which may justify the use of the term "front" even at that level. Particularly striking is the crowding of isotherms in the southwestern corner of the map, probably an effect of frontogenesis in a 300-mb col in the unmapped area west of Mexico. The 300-mb map under consideration is just tangent to a tropopause depression over the cold tongue of tropospheric air in the west. The map intersects the tropopause along the zone of lowest temperature across Labrador and northern Ontario. The temperature maximum east of the Hudson Bay cyclone is stratospheric. The cold air to its north is tropospheric and has been brought from lower latitudes as part of the warm sector shown in Fig. 9. On the 500-mb map, which is entirely tropospheric, the Hudson Bay center has a cold core with warmer surroundings both to the north and to the south.

The pressure minimum of the frontal wave at the Great Lakes continues up to 700 mb with some westward tilt, but at that level it has already shrunk so as to be a minor feature in the pressure field compared to

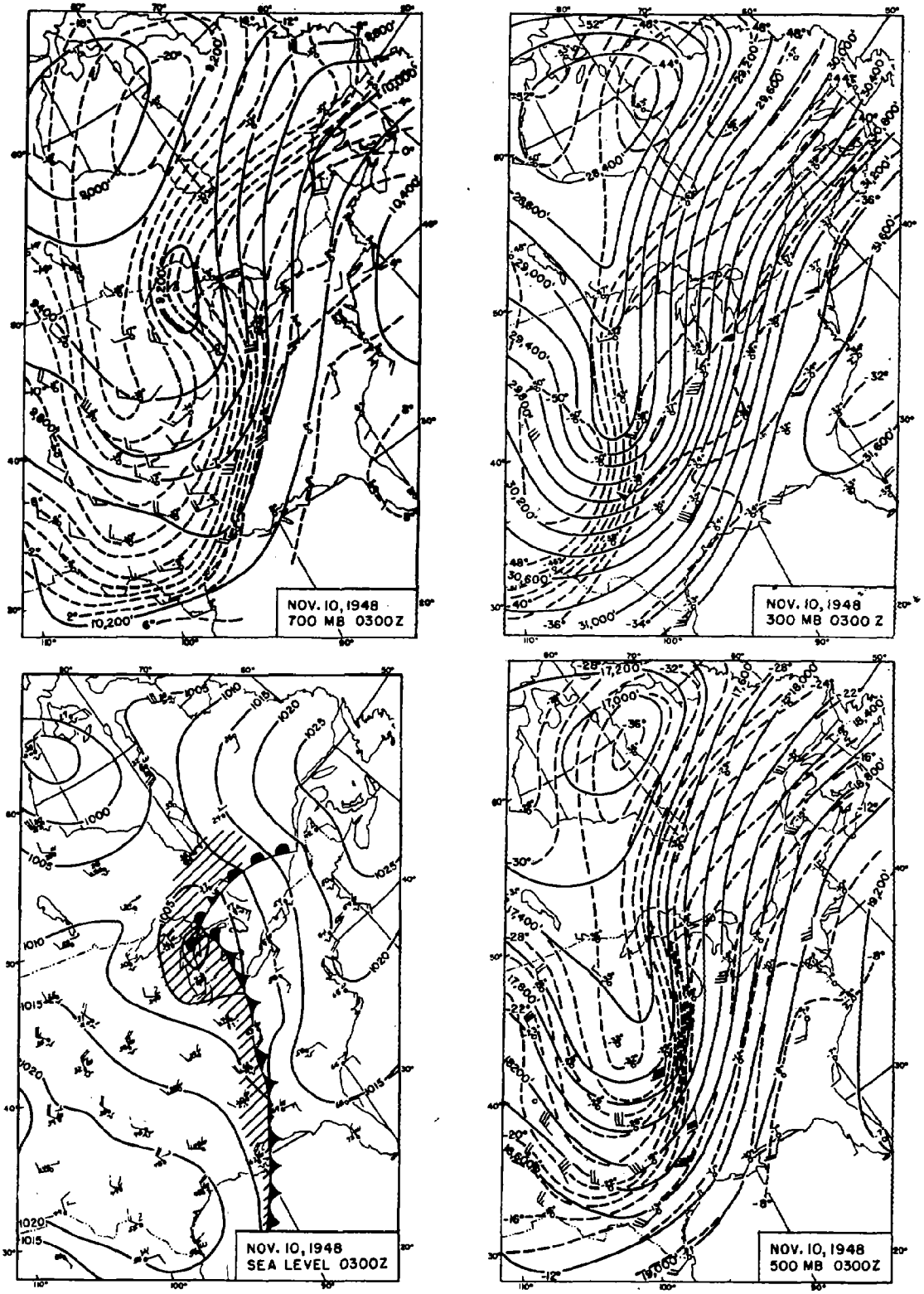

FIG. 14.—Structure of maturing frontal cyclone at sea level, 700 mb, 500 mb, and 300 mb, on November 10, 1948, 0300Z. Upper winds: Half barb 5 m sec^{-1}, full barb 10 m sec^{-1}, triangular barb 50 m sec^{-1}.

the old stationary Hudson Bay minimum. But the young cyclone over the Great Lakes has all the potentialities of development inherent in the solenoid field concentrated along the frontal wave all through the troposphere. As a hydrostatic consequence of the wave-shaped pattern of isotherms, the upper current above the closed center is likewise wave-shaped with an anticyclonic bend over the warm-front area of upgliding.

The frontal cyclone deepened at the rapid rate of 14 mb per twelve hours during November 10, and ended up as a storm center of 975 mb over northern Labrador on November 12. We shall briefly consider the application of the various theories of upper-air divergence which may claim to explain the deepening. Considering first the formation of the upper pressure crest which precedes the surface cyclone, we shall see the nature of the interplay between lower and upper layers. The fact that the upper pressure crest moves at a speed of only 9 m sec^{-1} in a current of 70–80 m sec^{-1} shows that the upper wave cannot be a free one. The time and place of the first appearance of the pressure crest on the 300-mb map (November 9, 0300Z) make it likely that the upper crest was formed by the upward motion connected with the beginning frontal upgliding in the nascent frontal wave. Once the upper wave is established, upper divergence will be located in the area between the preexisting upper pressure trough and the new upper pressure crest ahead of it. With the trough in north-northeast–south-southwest orientation and the pressure crest in northwest–southeast orientation, the half wave length between them shortens northward and makes the upper divergence particularly strong in that region. This is also the region where the rapid deepening of the frontal cyclone takes place. So far, the dynamics involved in the deepening process conform with the principles of Fig. 1. With that basic pattern accepted, we must also admit the existence of the following modifying processes.

The upper pressure crest is continually being fed from below by the rising motion in the front half of the cyclone and therefore is forced to maintain the same slow speed of propagation as the surface vortex. When the curvature of the anticyclonic bend of upper isobars becomes sufficiently strong, the fast upper current is unable to follow the isobars in gradient wind fashion, and horizontal divergence must result on both sides of the upper crest line (see p. 590). This component of upper divergence modifies the model in Fig. 1 in the sense of extending the pressure fall farther ahead of the surface center.

The upper-air divergence of the Ryd-Scherhag theories (p. 586) is also superimposed on the divergence and convergence inherent in the wave pattern. It can best be judged by comparing the geostrophic wind at two successive inflection points. The average geostrophic wind between the 30,000-ft and 29,000-ft contours at the inflection point southwest of the Great Lakes was 60 m sec^{-1}, and between the same contours at the inflection point over Labrador it was 42 m sec^{-1}. Therefore it can be concluded that the Great Lakes cyclone was situated under a "delta" of the upper current, and that an upper divergence pattern in the style of Fig. 8 would be superimposed. This upper pattern would tend to produce pressure falls in the northern half and pressure rises in the southern half of the delta. It may be counted in favor of this reasoning that the Great Lakes cyclone proceeded northeastward to northern Labrador and not along the 300-mb contours ahead of the storm which would have meant east-northeastward propagation.

The sample cyclone described above had its early development near the ground, where the frontal upgliding of the warm air and the downgliding of the cold were a direct consequence of the preceding frontogenesis. Such wave cyclogenesis is typical for all the frontogenetical areas of the middle and high latitudes. Another type of cyclogenesis occurs at times independently of any pre-existing low-level front. The cyclogenetic mechanism in that case seems to lie in the dynamic instability of the upper tropospheric westerlies, which leads to the meandering of the current and the subsequent formation of an upper cold low. Cyclogenesis of this kind is described by means of two synoptic examples in the following article by E. Palmén. In one example, that of November 4, 1946, the upper low did not reach a frontogenetical area, and did not extend down to the surface. In the other case, that of November 17–18, 1948, a frontal wave action can be discerned but, in contrast to the case of November 7–10, 1948, the wave motion started first in the upper troposphere and later extended to low levels.

CONCLUSION

Summing up our state of knowledge of extratropical cyclones, we may classify their formation as being due either to unstable frontal wave action or to unstable growth of an upper wave trough. A subsequent combination of both processes is quite frequent, and all the strongest cyclones on record seem to have that double origin. This article has dealt mainly with the unstable frontal wave action, which is in itself a large subject. The descriptive study of cyclogenesis and cyclone growth is carried out daily by all the weather forecasters of middle latitudes, and an adequate report on their experiences would have exceeded by far the scope of this article. The theoretical study of the model of frontal cyclogenesis has been the work of a small number of scholars of dynamical meteorology. Viewed in retrospect, the contribution of H. von Helmholtz to this field of research appears to be of outstanding importance and to represent the foundation upon which contemporary and future theories should build. The Helmholtzian concept of dynamic instability of the inertial motion in isentropic surfaces points out which properties of the atmospheric fields of mass and motion on a rotating earth are conducive to the growth of perturbations from infinitesimal to finite amplitudes; and it seems obvious that such a fundamental theoretical principle must have its applications to the early phases of the life cycle of cyclones. However, there is still a wide gap to be bridged between the existing theory of dynamic instability and the applications called

for in daily synoptic practice. Helmholtz considered only the background pattern of an atmosphere moving zonally at all longitudes. What synopticians need are the criteria of dynamic instability for large-scale atmospheric currents which are nonzonal and nonpermanent, because they are part of a slowly moving, long-wave pattern, but still offer the propitious environment for the quick growth of perturbations of cyclone size.

Once the frontal wave has occluded, dynamic instability in the Helmholtz sense is eliminated, because of the accomplished spread of cyclonic vorticity to the whole cyclonic area. Indirect effects of dynamic instability may, however, be brought to the cyclone from the neighboring upwind anticyclonic part of the upper-tropospheric westerlies. In the absence of such a rejuvenating influence, the cyclone is left to decay by frictional inflow at the surface unopposed by deepening effects in the upper troposphere. This sketch of the last part of the life cycle of cyclones is even less intimately related to exact dynamic theories than is the existing theory of frontal cyclogenesis. The most hopeful approach to a solution of the problems of the old cyclone is most likely to be through the study of the energy transformations in the cyclone and its farther environment. The major old cyclones occupy such big fractions of the volume and weight of the atmosphere that the "farther environment" must be taken to mean the whole hemispherical circulation.

REFERENCES

1. Bergeron, T., "Über die dreidimensional verknüpfende Wetteranalyse." *Geofys. Publ.*, Vol. 5, No. 6 (1928).
2. Bjerknes, J., "Theorie der aussertropischen Zyklonenbildung." *Meteor. Z.*, 54: 462–466 (1937).
3. —— and Holmboe, J., "On the Theory of Cyclones." *J. Meteor.*, 1: 1–22 (1944).
4. Charney, J. G., "The Dynamics of Long Waves in a Baroclinic Westerly Current." *J. Meteor.*, 4: 135–162 (1947).
5. Cressman, G. P., "On the Forecasting of Long Waves in the Upper Westerlies." *J. Meteor.*, 5: 44–57 (1948).
6. Eliassen, A., "The Quasi-static Equations of Motion with Pressure as Independent Variable." *Geofys. Publ.*, Vol. 17, No. 3, pp. 30–34 (1949).
7. Ertel, H., Jaw, J.-J., und Li, S.-z., "Tensorielle Theorie der Stabilität." *Meteor. Z.*, 58: 389–392 (1941).
8. Fjørtoft, R., "On the Deepening of a Polar Front Cyclone." *Meteor. Ann.*, 1: 1–44 (1942).
9. —— "On the Frontogenesis and Cyclogenesis in the Atmosphere. Part I—On the Stability of the Stationary Circular Vortex." *Geofys. Publ.*, Vol. 16, No. 5 (1946).
10. Haurwitz, B., "The Motion of Atmospheric Disturbances." *J. mar. Res.*, 3: 35–50 (1940).
11. —— *Dynamic Meteorology.* New York, McGraw, 1941. (See p. 234)
12. Helmholtz, H. v., "Über atmosphärische Bewegungen." *Meteor. Z.*, 5: 329–340 (1888).
13. Hesselberg, T., und Friedmann, A., "Grössenordnung der meteorologischen Elemente." *Veröff. geophys. Inst. Univ. Lpz.*, 1: 147–173 (1914).
14. Höiland, E., "On the Interpretation and Application of the Circulation Theorems of V. Bjerknes." *Arch. Math. Naturv.*, 42: 25–57 (1939).
15. —— "On the Stability of the Circular Vortex." *Avh. norske VidenskAkad.*, No. 11 (1941).
16. Holmboe, J., and others, *Dynamic Meteorology.* New York, Wiley, 1945. (See pp. 324–325)
17. Holmboe, J., "On Dynamic Stability of Zonal Currents." *J. mar. Res.*, 7: 163–174 (1948).
18. Kleinschmidt, E., "Stabilitätstheorie des geostrophischen Windfeldes." *Ann. Hydrogr., Berl.*, 69: 305–325 (1941).
19. —— "Zur Theorie der labilen Anordnung." *Meteor. Z.*, 58: 157–163 (1941).
20. Miller, J. E., "Studies of Large-Scale Vertical Motions of the Atmosphere." *Meteor. Pap. N. Y. Univ.*, Vol. 1, No. 1, 49 pp. (1948).
21. Moltschanow, P., "Bedingungen des Gleichgewichts und der Stabilität der Luftmassen nach der Horizontalen und der Vertikalen." *Petermanns Mitt.*, Erg. 47, Heft 216, SS. 62–67 (1933).
22. Palmén, E., "Aerologische Untersuchungen der atmosphärischen Störungen." *Acta Soc. Sci. fenn.*, Phys. Math., Vol. 7, No. 6 (1933).
23. —— "On the Distribution of Temperature and Wind in the Upper Westerlies." *J. Meteor.*, 5: 20–27 (1948).
24. —— and Newton, C. W., "A Study of the Mean Wind and Temperature Distribution in the Vicinity of the Polar Front in Winter." *J. Meteor.*, 5: 220–226 (1948).
25. Petterssen, S., *Weather Analysis and Forecasting.* New York, McGraw, 1940. (See pp. 238–248)
26. Rossby, C.-G., and Collaborators, "Relation between Variations in the Intensity of the Zonal Circulation of the Atmosphere and the Displacements of the Semi-permanent Centers of Action." *J. mar. Res.*, 2: 38–55 (1939).
27. Rossby, C.-G., "Kinematic and Hydrostatic Properties of Certain Long Waves in the Westerlies." *Dept. Meteor. Univ. Chicago, Misc. Rep.* No. 5 (1942).
28. Ryd, V. H., "Meteorological Problems, II—Travelling Cyclones." *Medd. danske meteor. Inst.*, No. 5, 124 pp. (1923).
29. —— "The Energy of the Winds." *Medd. danske meteor. Inst.*, No. 7 (1927).
30. Scherhag, R., *Neue Methoden der Wetteranalyse und Wetterprognose.* Berlin, Springer, 1948. (See pp. 184–187)
31. Solberg, H., "Le mouvement d'inertie de l'atmosphère stable et son rôle dans la théorie des cyclones." *P. V. Météor. Un. géod. géophys. int.*, Edimbourg, 1936. II, pp. 66–82 (1939).
32. Van Mieghem, J., "Forme intrinsèque du critère d'instabilité dynamique de E. Kleinschmidt." *Bull. Acad. Belg. Cl. Sci.*, 5e sér., 30: 19–34 (1944). (For several subsequent papers see references in "Hydrodynamic Instability" by J. Van Mieghem in this Compendium.)


NOAA
NATIONAL OCEANIC AND ATMOSPHERIC ADMINISTRATION
U.S. DEPARTMENT OF COMMERCE